EDQNM model of a passive scalar with a uniform mean gradient

Stacy Herr[a)]
Department of Chemical Engineering, The Pennsylvania State University, 115 Fenske Laboratory, University Park, Pennsylvania 16802

Lian-Ping Wang
Department of Mechanical Engineering, University of Delaware, Newark, Delaware 19716

Lance R. Collins[b)]
Department of Chemical Engineering, The Pennsylvania State University, 118-B Fenske Laboratory, University Park, Pennsylvania 16802

(Received 1 September 1995; accepted 17 January 1996)

Dynamic equations for the scalar autocorrelation and scalar-velocity cross correlation spectra have been derived for a passive scalar with a uniform mean gradient using the Eddy Damped Quasi Normal Markovian (EDQNM) theory. The presence of a mean gradient in the scalar field makes all correlations involving the scalar axisymmetric with respect to the axis pointing in the direction of the mean gradient. Equivalently, all scalar spectra will be functions of the wave number k and the cosine of the azimuthal angle designated as μ. In spite of this complication, it is shown that the cross correlation vector can be completely characterized by a single scalar function $Q(k)$. The scalar autocorrelation spectrum, in contrast, has an unknown dependence on μ. However, this dependency can be expressed as an infinite sum of Legendre polynomials of μ, as first suggested by Herring [Phys. Fluids **17**, 859 (1974)]. Furthermore, since the scalar field is initially zero, terms beyond the second order of the Legendre expansion are shown to be exactly zero. The energy, scalar autocorrelation, and scalar-velocity cross correlation were solved numerically from the EDQNM equations and compared to results from direct numerical simulations. The results show that the EDQNM theory is effective in describing single-point and spectral statistics of a passive scalar in the presence of a mean gradient. © *1996 American Institute of Physics.* [S1070-6631(96)00205-X]

I. INTRODUCTION

It has long been recognized that the behavior of a passive scalar differs significantly from that of the velocity field for profound and fundamental reasons. Close examination of the two fields shows that while the velocity field organizes itself into long tubes at high vorticity, the scalar field more closely resembles a rolled up pancake at equivalent levels of scalar dissipation. The origin of this difference can be traced to the convective term in the transport of each property, which in the case of the scalar is simply the velocity dotted into the scalar gradient while advection in the momentum equation is modified by the pressure field. This subtle change is responsible for significant qualitative differences in the features of the two fields. Recently the scalar field has received increased experimental attention[1–5] as investigators continue to catalog the important characteristics of the scalar field and its derivatives. Indeed, the scalar in the presence of a uniform mean gradient has been the subject of several recent articles.[6–10] One question that can be asked is whether theories that have been successful in describing the behavior of the turbulent energy can be applied to the scalar. We consider this question in the present study by applying the Eddy Damped Quasi-Normal Markovian theory (EDQNM) to the dynamics of a passive scalar with a uniform mean gradient in stationary isotropic turbulence. Our results indicate that although one can postulate several objections to a quasinormal theory for a passive scalar, it appears to represent the data from direct numerical simulations reasonably well over the parameter range considered.

There have been a wide range of experimental investigations of a passive scalar with a uniform mean gradient over the years. For example, the study by Tavoularis and Corrsin[11,12] introduced a mean gradient in temperature across grid-generated turbulence and measured the spectrum of scalar fluctuations that resulted. More recently, Warhaft and several co-workers have considered in great detail the behavior of a passive scalar in a series of papers.[1–5] Classical scaling arguments set forth by Kolmogorov[13] for the energy spectrum and subsequently by Obukhov[14] and Corrsin[15] for the scalar spectrum (hereafter referred to as KOC) established that the scalar spectrum should have the following form in the so-called inertial-convective range:[16]

$$E_B(k) = \beta \epsilon^{-1/3} \chi k^{-5/3}, \tag{1}$$

where $E_B(k)$ is the three-dimensional scalar spectrum, ϵ and χ are the average rate of dissipation of energy and scalar, respectively, and β is a universal constant (according to the theory). Jayesh *et al.*[3] observed that the presence of a mean gradient improved the agreement between the observed scalar spectrum and the KOC theory. Indeed, quantitative *disagreement* with KOC theory has occurred only for the case of an *isotropic* decaying scalar introduced downstream from the grid-generated turbulence. The explanation appears to be that at moderate to low Reynolds numbers there are systematic deviations from KOC unless there are strong correlations between the initial velocity and scalar fluctuations. Scalar

[a)]Present address: Occidental Chemical Corporation, Ashtabula, Ohio.
[b)]Electronic mail: LXC12@CAC.PSU.EDU.

 1070-6631/96/8(6)/1588/21/$10.00

fluctuations that arise from the presence of a mean gradient are, by definition, strongly correlated with the velocity field, hence KOC scaling is valid for that case. This is confirmed by most of the experimental investigations and our theoretical results. One aspect that was not discussed by Jayesh *et al.*[3] but has been discussed by others (e.g., Ref. 6) is how the change from isotropy to axisymmetry manifests on the scalar spectrum. This is one focus of the present analysis.

From the preceding discussion, you might conclude that the scalar field can be completely characterized by the simple KOC theory (assuming the Reynolds number is sufficiently large); however, closer examination reveals that there are significant discrepancies that still require explanation. For example, measurements of the probability density function (pdf) for the scalar and scalar gradient show well-defined exponential tails, particularly at large positive deviations from the mean[2,4,5,8,17] (as opposed to the Gaussian form implied by KOC). These tails appear to be connected to rampcliff structures in the scalar field that result from the anisotropy introduced by the presence of the mean gradient. A comprehensive discussion of the exponential tails has been given by Jayesh and Warhaft,[4] Tong and Warhaft,[2] and Pumir.[6] Recently a theory has been developed by Pumir *et al.*[7] to explain these structures. Given the strongly non-Gaussian character of the scalar fluctuations, the question becomes whether theories based on Gaussian or near-Gaussian statistics have any range of validity for a scalar with a uniform mean gradient.

EDQNM theory[18] has been used to describe a variety of turbulent systems, including the classical studies of the energy and isotropic scalar spectrum,[19,20] to more exotic problems involving mean flow inhomogeneities.[21–25] The theory relies on near Gaussian statistics for all fourth-order moments. As noted above, experimental measurements of *isotropic* scalar fluctuations have pdfs that are nearly Gaussian supporting the theoretical approach, however, the presence of a mean gradient appears to make this assumption somewhat more tenuous. Our results indicate that the EDQNM theory can successfully represent the spectrum of a passive scalar with a mean gradient, despite these objections. An explanation may be that the exponential tails in the pdf of the scalar fluctuations are low-probability events, and as such, while they may alter the higher-order statistics significantly, their contribution to second-order statistics is negligible. Thus, the important features of the modeled fourth-order scalar statistics are represented sufficiently well by the EDQNM approximations, such that the second-order correlations are predicted accurately. For example, it may be sufficient that the pdf be nearly symmetric ensuring that odd-order moments are small as compared to even-order moments. In addition, built in corrections for the effect of *cumulants* may also compensate for the non-Gaussian statistics in the case of a mean gradient.

In this paper we consider the dynamics of a passive scalar with a uniform mean gradient advected by stationary, isotropic turbulence. The presence of a mean gradient reduces the symmetry of all correlations involving the scalar from isotropic (as found for a freely decaying scalar) to axisymmetric. As a result, the theoretical treatment of the scalar field must be generalized to take this into account. This apparently minor extension of the EDQNM theory significantly increases the complexity of the computation, although the final form of the integral equation remains essentially the same as that for an isotropic scalar field. The approach taken is equivalent to the one described originally by Batchelor[26] and Chandreshekar,[27] and more recently by Nakauchi[24] and Herring[25] in studies of sheared turbulence. In the analysis by Herring, the geometric dependence on the angle to the mean gradient was accounted for by expanding the functions in a polynomial series in cosines of that angle. We adopt a similar approach. In addition, comparisons of the results from the EDQNM theory are made with direct numerical simulations performed on a 128^3 lattice over very long times (60 eddy turnover times). This allowed us to fix the two unknown coefficients that result from the theory.

The paper is organized as follows. The equations of motion are summarized in Sec. II, followed by derivations of the EDQNM model equations for the energy spectrum (Sec. III), velocity-scalar spectrum (Sec. IV) and scalar autocorrelation spectrum (Sec. V). The cross correlation is considered first because many of its terms are duplicated in the autocorrelation equation. In Sec. VI we give a brief description of the numerical method used to solve the integrodifferential equations that result from the EDQNM analysis. Details of the direct numerical simulations are then provided in Sec. VII. Model results, discussion, and comparisons between direct numerical simulations and the EDQNM model are given in Sec. VIII, followed by conclusions in Sec. IX.

II. GOVERNING EQUATIONS

The fluid is considered to be incompressible with a constant kinematic viscosity, thus the governing equations are

$$\frac{\partial u_i}{\partial x_i} = 0, \tag{2a}$$

$$\frac{\partial u_i}{\partial t} + u_j \frac{\partial u_i}{\partial x_j} + \frac{1}{\rho}\frac{\partial p}{\partial x_i} = \nu \frac{\partial^2 u_i}{\partial x_j^2} + F_i, \tag{2b}$$

where u_i is the fluctuating fluid velocity (there is no mean flow), p is the pressure, ρ is the density, ν is the kinematic viscosity, and F_i is a solenoidal forcing function introduced to maintain stationary turbulence. In the simulations, forcing is introduced over a narrow band of small wave numbers under the assumption that its net effect on the turbulent energy transfer process is negligible. Consequently, the effect of the forcing is modeled as a source term at small wave numbers, and its influence on energy transfer is neglected (although it should be noted that our results provide evidence that the forcing function enhances the rate of transfer over the forcing range—see Sec. VIII A for details). The precise form of the forcing in the EDQNM model will be discussed in greater detail in Sec. III. It is possible and convenient to eliminate the pressure from Eqs. (2a) and (2b) by taking advantage of the continuity relationship.[28] The resulting expression is

$$\frac{\partial u_i}{\partial t} + \frac{1}{2} P_{ijm} u_j u_n = \nu \frac{\partial^2 u_i}{\partial x_j^2} + F_i, \tag{3a}$$

where the operator P_{ijm} is given by

$$P_{ijm}=\delta_{ij}\frac{\partial}{\partial x_m}+\delta_{im}\frac{\partial}{\partial x_j}+\frac{2}{\nabla^2}\frac{\partial^3}{\partial x_i\,\partial x_j\,\partial x_m}. \tag{3b}$$

The transport equation for a passive scalar with constant physical properties in an incompressible system is shown below:

$$\frac{\partial\Phi}{\partial t}+u_j\frac{\partial\Phi}{\partial x_j}=\kappa\frac{\partial^2\Phi}{\partial x_j^2}. \tag{4}$$

Without loss of generality, the scalar is assumed to have a uniform mean gradient with a magnitude Γ pointing in the $\mathbf{e}_3$ direction ($\mathbf{e}_3$ is a unit normal pointing in the x_3 direction). The system is still homogeneous under this circumstance, although correlations involving the scalar field will no longer be isotropic. The resulting governing equation for the scalar fluctuation defined as $\Phi'=\underline{\Phi}-\Phi$ (where Φ is the mean scalar concentration given by $\Phi=\Gamma x_3$) is as follows:

$$\frac{\partial\Phi'}{\partial t}+u_j\frac{\partial\Phi'}{\partial x_j}+u_3\Gamma=\kappa\frac{\partial^2\Phi'}{\partial x_j^2}. \tag{5}$$

At this stage, it is convenient to nondimensionalize the equations based on the integral length scale L, the turbulence intensity $U_{\rm rms}$, the large eddy turnover time $L/U_{\rm rms}$, and the characteristic scalar fluctuation ΓL, resulting in the following:

$$\frac{\partial u_i}{\partial t}+\frac{1}{2}P_{ijm}u_ju_m=\frac{1}{R_L}\frac{\partial^2u_i}{\partial x_j^2}+F_i, \tag{6a}$$

$$\frac{\partial\Phi'}{\partial t}+u_j\frac{\partial\Phi'}{\partial x_j}+u_3=\frac{1}{\mathrm{Pe}}\frac{\partial^2\Phi'}{\partial x_j^2}, \tag{6b}$$

where the Reynolds number is $R_L=U_{\rm rms}L/\nu$, the Peclet number is $\mathrm{Pe}=R_LP$, and the Prandtl number is defined by $P=\nu/\kappa$. Note, for the sake of maintaining a manageable nomenclature, that we have designated the nondimensional variables with the same symbols as the dimensional ones, with the understanding that hereafter all variables should be assumed to be nondimensional unless specified otherwise. Furthermore, it should be noted that the only parameters that remain in the problem are R_L and P because the magnitude of the mean gradient is effectively scaled out of the problem. Eqs. (6a) and (6b) now become the basic equations from which the spectral model shall be derived.

III. EDQNM THEORY FOR ENERGY

Derivations of the EDQNM closure for the energy spectrum have been discussed in numerous publications; hence we will only highlight the relevant features for the present calculations. The reader is referred to the book by Lesieur[28] for a more detailed description. The energy spectrum is most easily derived from the two-point Reynolds stress shown below:

$$R_{ij}(\mathbf{x}_1,\mathbf{x}_2)=\overline{u_i(\mathbf{x}_1)u_j(\mathbf{x}_2)}. \tag{7}$$

Forward and reverse Fourier transforms are designated with the following convention:

$$R_{ij}(\mathbf{k},\mathbf{p})=\int\int R_{ij}(\mathbf{x}_1,\mathbf{x}_2)e^{-i(\mathbf{k}\cdot\mathbf{x}_1+\mathbf{p}\cdot\mathbf{x}_2)}d\mathbf{x}_1\,d\mathbf{x}_2, \tag{8a}$$

$$R_{ij}(\mathbf{x}_1,\mathbf{x}_2)=\int\int R_{ij}(\mathbf{k},\mathbf{p})e^{+i(\mathbf{k}\cdot\mathbf{x}_1+\mathbf{p}\cdot\mathbf{x}_2)}\not{d}\mathbf{k}\,\not{d}\mathbf{p}, \tag{8b}$$

where $\not{d}\mathbf{k}$ and $\not{d}\mathbf{p}$ refer to $d\mathbf{k}/(2\pi)^3$ and $d\mathbf{p}/(2\pi)^3$, respectively. [Fourier transforms of higher-order correlations are obtained from a straightforward generalization of Eqs. (8a) and (8b).] It can be shown that for a homogeneous energy field, the Reynolds stress $R_{ij}(\mathbf{k},\mathbf{p})$ is proportional to the three-dimensional Dirac delta function $\hat{\delta}(\mathbf{k}+\mathbf{p})$. Furthermore, the assumption of isotropy and no helicity implies

$$R_{ij}(\mathbf{k},\mathbf{p})=\hat{\delta}(\mathbf{k}+\mathbf{p})R(k)P_{ij}(\mathbf{k}), \tag{9a}$$

where

$$P_{ij}(\mathbf{k})=\delta_{ij}-\frac{k_ik_j}{k^2} \tag{9b}$$

is the projection operator and δ_{ij} refers to the Kronecker delta function. [Note that the energy spectrum, often designated by $E(k)$, is related to $R(k)$ by $E(k)=k^2R(k)/2\pi^2$.] Based on the definitions shown in Eqs. (8a) and (8b), it can be shown that the turbulent intensity (i.e., root mean square of the velocity fluctuations) is related to $R(k)$ by

$$U_{\rm rms}^2=\frac{1}{3\pi^2}\int_0^\infty R(k)k^2\,dk. \tag{10}$$

As shown by Lesieur,[28] the EDQNM model transport equation for $R(k)$ for a *statistically stationary* turbulent system is as follows:

$$2R_L^{-1}k^2R(k)=\int_\Delta\int\Theta_R^{kpq}[V_1R(q)R(p)+V_2R(q)R(k)]dp\,dq+F(k), \tag{11a}$$

where

$$V_1=\frac{qp^2}{2\pi^2}[xy-z^3], \tag{11b}$$

$$V_2=-V_1, \tag{11c}$$

$$\Theta_R^{kpq}=\frac{1}{\mu_R^{kpq}}, \tag{11d}$$

while the eddy damping coefficient μ_R^{kpq} is given by

$$\mu_R^{kpq}=c_1(\mu_k+\mu_p+\mu_q)+R_L^{-1}(k^2+p^2+q^2) \tag{11e}$$

and the time scale μ_k is determined from the following integral:

$$\mu_k=\frac{1}{\sqrt{2}\pi}\left(\int_0^k s^4R(s)ds\right)^{1/2}. \tag{11f}$$

The coefficients x, y, and z refer to the cosines of the interior angles of the triad, and are defined as shown below:

$$x\equiv\frac{\mathbf{p}\cdot\mathbf{q}}{pq}=\frac{k^2-p^2-q^2}{2pq}, \tag{11g}$$

$$y \equiv \frac{\mathbf{k}\cdot\mathbf{q}}{kq} = \frac{p^2 - k^2 - q^2}{2kq}, \tag{11h}$$

$$z \equiv \frac{\mathbf{k}\cdot\mathbf{p}}{kp} = \frac{q^2 - k^2 - p^2}{2kp}. \tag{11i}$$

The constant c_1 is usually assigned the value 0.36 to ensure that the energy spectrum at infinite Reynolds number obeys the classical Kolmogorov scaling argument.[29] The forcing term is assumed to have the form

$$F(k) = \begin{cases} F_k, & k \leqslant 2, \\ 0, & k > 2, \end{cases}$$

where the constants F_1 and F_2 are set to match the conditions of the direct numerical simulations (see Sec. VIII for details).

IV. SCALAR-VELOCITY CROSS CORRELATION

We must recognize from the outset that the variable Φ', which is isotropic for the decaying scalar case, is now *axisymmetric* (about the $\mathbf{e}_3$ axis) in the present system. It therefore follows that all two-point correlations that involve Φ' must be functions of the separation distance *and* the angle between the separation vector and the mean gradient. The correlations of interest to the present study are the scalar autocorrelation $B(\mathbf{x}_1,\mathbf{x}_2) = \overline{\Phi'(\mathbf{x}_1)\Phi'(\mathbf{x}_2)}$ and scalar-velocity cross correlation, $Q_i(\mathbf{x}_1,\mathbf{x}_2) = \overline{u_i(\mathbf{x}_1)\Phi'(\mathbf{x}_2)}$. The objective of this section is to derive a transport equation for the Fourier transform of $Q_i(\mathbf{x}_1,\mathbf{x}_2)$ shown below:

$$Q_i(\mathbf{k},\mathbf{p}) = \int\int Q_i(\mathbf{x}_1,\mathbf{x}_2) e^{-i(\mathbf{k}\cdot\mathbf{x}_1 + \mathbf{p}\cdot\mathbf{x}_2)}\, d\mathbf{x}_1\, d\mathbf{x}_2, \tag{12}$$

in closed form.

Homogeneity, axisymmetry, and the continuity relationship force the cross-correlation vector to have the following form;

$$Q_i(\mathbf{k},\mathbf{p}) = \hat{\delta}(\mathbf{k}+\mathbf{p}) Q(k) P_{i3}(\mathbf{k}), \tag{13}$$

thus reducing the model to a scalar equation for the function $Q(k)$. In general, the scalar Q is a function of the wave number k, and μ, the cosine of the angle between the wave vector $\mathbf{k}$ and the direction of the mean gradient, i.e., $\mu \equiv \mathbf{k}\cdot\mathbf{e}_3/|\mathbf{k}|$ However, in the present application, this angle dependence is not observed for reasons related to the initial conditions of the scalar field. Scalar fluctuations (i.e., Φ') are initially zero and build up thereafter because of the presence of the mean gradient. As a result, the scalar function $Q(k)$, whose source term is isotropic, remains independent of μ for all time. More general initializations may introduce anisotropy in Q, however, those circumstances are beyond the scope of the present analysis. Incidentally, any anisotropy introduced by the initial conditions will decay in time and therefore will not affect the steady-state solutions.

Physically, the single-point cross-correlation vector $Q_i \equiv \overline{u_i\Phi'}$ is the turbulent flux of scalar passing through the system due to the random velocity fluctuations. The only nonzero component of this vector in the present system lies in the direction of the mean gradient, i.e. $Q_3 \equiv \overline{u_3\Phi'}$. From the definitions of the spectra [Eqs. (12) and (13)], Q_3 is given by

$$Q_3 = \overline{u_3\Phi'} = \frac{1}{3\pi^2} \int_0^\infty Q(k) k^2\, dk. \tag{14}$$

A. Exact equation

We begin with the transport equation for $Q_i(\mathbf{x}_1,\mathbf{x}_2)$, which is found by manipulating the governing equations for the velocity and scalar fluctuations [Eqs. (6a) and (6b)],

$$\left(\frac{\partial}{\partial t} - R_L^{-1}\nabla_1^2 - \mathrm{Pe}^{-1}\,\nabla_2^2\right) Q_i(\mathbf{x}_1,\mathbf{x}_2)$$
$$= -\frac{\partial}{\partial x_{1n}} P_{ijn}(\mathbf{x}_1) T_{jn}(\mathbf{x}_1,\mathbf{x}_1,\mathbf{x}_2)$$
$$- \frac{\partial}{\partial x_{2n}} T_{in}(\mathbf{x}_1,\mathbf{x}_2,\mathbf{x}_2) - R_{i3}(\mathbf{x}_1,\mathbf{x}_2), \tag{15a}$$

where

$$T_{jn}(\mathbf{x}_1,\mathbf{x}_2,\mathbf{x}_3) = \overline{u_j(\mathbf{x}_1) u_n(\mathbf{x}_2)\Phi'(\mathbf{x}_3)}. \tag{15b}$$

The operators ∇_1^2 and ∇_2^2 signify Laplacian derivatives with respect to $\mathbf{x}_1$ and $\mathbf{x}_2$ respectively. Fourier Transforming the above equation and taking advantage of Eq. (13) yields

$$\left(\frac{\partial}{\partial t} + (R_L^{-1} + \mathrm{Pe}^{-1})k^2\right) Q(k)$$
$$= + \frac{i}{(1-\mu^2)} \int\int \left(k_n P_{j3}(\mathbf{k}) T_{jn}(\mathbf{k},\mathbf{p},\mathbf{q}) \right.$$
$$\left. + \frac{1}{2} P_{3jn}(\mathbf{k}) T_{jn}(\mathbf{q},\mathbf{p},\mathbf{k}) \right) d\mathbf{p}\, d\mathbf{q} - R(k), \tag{16}$$

where the third-order tensor $P_{ijm}(\mathbf{k}) = k_m P_{ij}(\mathbf{k}) + k_j P_{im}(\mathbf{k})$. The nonlinear integral in Eq. (16) shall be approximated by using the EDQNM theory.

B. EDQNM closure and final equation for $Q(k)$

Equation 16 is an exact transport equation for the spectrum $Q(k)$, however, it involves an unknown triple correlation $T_{jn}(\mathbf{k},\mathbf{p},\mathbf{q})$. The approximate solution for $T_{jn}(\mathbf{k},\mathbf{p},\mathbf{q})$ based on a rigorous application of EDQNM theory is as follows (see Appendix A for details):

$$T_{jn}(\mathbf{k},\mathbf{p},\mathbf{q}) = -i\hat{\delta}(\mathbf{k}+\mathbf{p}+\mathbf{q})\Theta_T^{kpq}\{-\Theta_R^{kqp}[D_{3jn}^{qkp} R(k)R(p)$$
$$+ D_{nj3}^{pkq} R(k)R(q) + D_{j3n}^{kqp} R(p)R(q)]$$
$$+ C_{nj}^{qpk} R(p)Q(k) + D_{n3j}^{pqk} R(k)Q(q)$$
$$+ D_{jn3}^{kpq} R(p)Q(q) + C_{jn}^{qkp} R(k)Q(p)\}, \tag{17a}$$

where

$$C_{ij}^{kpq} = C_{ij}(\mathbf{k},\mathbf{p},\mathbf{q}) = k_a P_{ia}(\mathbf{p}) P_{j3}(\mathbf{q}), \tag{17b}$$

$$D_{ijm}^{kpq} = D_{ijm}(\mathbf{k},\mathbf{p},\mathbf{q}) = P_{iab}(\mathbf{k}) P_{aj}(\mathbf{p}) P_{bm}(\mathbf{q}), \tag{17c}$$

$$\Theta_T^{kpq}=\frac{1-e^{-\mu_T^{kpq}t}}{\mu_T^{kpq}}, \tag{17d}$$

$$\mu_T^{kpq}=c_2(\mu_k+\mu_p)+c_3\mu_q+R_L^{-1}(k^2+p^2)+\mathrm{Pe}^{-1}\ q^2. \tag{17e}$$

The geometric factors C_{ij}^{kpq} and D_{ijm}^{kpq} arise from substituting the tensor relationships for the Reynolds stress [Eqs. (9a) and (9b)] and cross correlation [Eq. (13)] into the expression for T_{jn} $(\mathbf{k},\mathbf{p},\mathbf{q})$. Note that the subscripts in the geometric factors [Eqs. (17b) and (17c)] indicate the indices of the tensor while the superscripts are a shorthand notation of the wave vector dependence. In previous EDQNM applications, the coefficients arising from the eddy damping terms (c_2 and c_3) have been constrained by a known asymptotic form for the spectrum valid at high Reynolds numbers, however, in this case, the asymptotic form of the cross-correlation spectrum is not known *a priori*. Instead, the coefficients c_2 and c_3 were chosen to match the results from the numerical simulations (see Sec. VIII for details).

Substituting Eqs. (17a)–(17e) into Eq. (16) yields a closed form transport equation for $Q(k)$. The nonlinear convolution integral over the wave vectors $\mathbf{p}$ and $\mathbf{q}$ can then be mathematically converted into an integral over the scalar wave numbers p and q. The details are given in Appendix B. Upon performing the integral over the angle ϕ_q analytically (see Appendix B for the definition of ϕ_q), a common factor of $(1-\mu^2)$ emerges throughout the equation. This factor is then canceled out, yielding the following integrodifferential equation for $Q(k)$:

$$\begin{aligned}\left(\frac{\partial}{\partial t}+(R_L^{-1}+\mathrm{Pe}^{-1})k^2\right)Q(k)=&-R(k)+\int_\Delta\int \Theta_T^{kpq}\{-\Theta_R^{kqp}[H_1R(k)R(p)+H_2R(k)R(q)+H_3R(p)R(q)]\\&+H_4R(p)Q(k)+H_5R(k)Q(q)+H_6R(p)Q(q)+H_7R(k)Q(p)\}\\&+\tfrac{1}{2}\Theta_T^{qpk}\{-\Theta_R^{qkp}[J_1R(k)R(p)+J_2R(k)R(q)+J_3R(p)R(q)]+J_4R(q)Q(k)\\&+J_5R(p)Q(q)+J_6R(q)Q(p)+J_7R(p)Q(k)\}dp\ dq.\end{aligned} \tag{18}$$

The 14 geometric cofactors H_1-H_7 and J_1-J_7 are summarized in Table I. Note that all coefficients are functions of the magnitudes of the wave numbers k, p, and q only. They are expressed in terms of x, y, and z, the cosines of the interior angles of the triad, which, in turn, can be related to the magnitudes of the wave numbers through the law of cosines [see Eqs. (11g)–(11i)].

V. SCALAR AUTOCORRELATION

The procedure for deriving the transport equation for the autocorrelation is equivalent to the one used for the cross correlation described in the previous section. The scalar autocorrelation $B(\mathbf{x}_1,\mathbf{x}_2)=\overline{\Phi'(\mathbf{x}_1)\Phi'(\mathbf{x}_2)}$, like the cross correlation, is axisymmetric with respect to the $\mathbf{e}_3$ direction. The Fourier transform of $B(\mathbf{x}_1,\mathbf{x}_2)$ is defined as

$$B(\mathbf{k},\mathbf{p})=\int\int B(\mathbf{x}_1,\mathbf{x}_2)e^{-i(\mathbf{k}\cdot\mathbf{x}_1+\mathbf{p}\cdot\mathbf{x}_2)}\ d\mathbf{x}_1\ d\mathbf{x}_2, \tag{19}$$

however homogeneity and axisymmetry reduce $B(\mathbf{k},\mathbf{p})$ to the following:

$$B(\mathbf{k},\mathbf{p})=\hat{\delta}(\mathbf{k}+\mathbf{p})2B(k,\mu). \tag{20}$$

It should be noted that the root mean square of the scalar fluctuations, $\Phi_{\mathrm{rms}}\equiv\sqrt{\overline{\Phi'^2}}$ is related to $B(k,\mu)$ by

$$\Phi_{\mathrm{rms}}^2=\frac{1}{2\pi^2}\int_0^\infty\int_{-1}^1 B(k,\mu)k^2\ d\mu\ dk. \tag{21}$$

A transport equation for $B(k,\mu)$ is derived below.

A. Exact equation

The transport equation for $B(\mathbf{x}_1,\mathbf{x}_2)$ is found by manipulating Eq. (6b), yielding

$$\begin{aligned}\left(\frac{\partial}{\partial t}-\mathrm{Pe}^{-1}(\nabla_1^2+\nabla_2^2)\right)&B(\mathbf{x}_1,\mathbf{x}_2)\\&=-\frac{\partial}{\partial x_{1n}}M_n(\mathbf{x}_1,\mathbf{x}_1,\mathbf{x}_2)-\frac{\partial}{\partial x_{2n}}M_n(\mathbf{x}_2,\mathbf{x}_1,\mathbf{x}_2)\\&\quad-Q_3(\mathbf{x}_1,\mathbf{x}_2)-Q_3(\mathbf{x}_2,\mathbf{x}_1),\end{aligned} \tag{22a}$$

where

$$M_n(\mathbf{x}_1,\mathbf{x}_2,\mathbf{x}_3)\equiv\overline{u_n(\mathbf{x}_1)\Phi'(\mathbf{x}_2)\Phi'(\mathbf{x}_3)}. \tag{22b}$$

Transforming Eq. (22a) yields

$$\begin{aligned}\left(\frac{\partial}{\partial t}+\mathrm{Pe}^{-1}(k^2+p^2)\right)&B(\mathbf{k},\mathbf{p})\\&=-i\hat{\delta}(\mathbf{k}+\mathbf{p})\int\int[k_nM_n(-\mathbf{p},\mathbf{p},-\mathbf{q})\\&\quad+p_nM_n(\mathbf{p},\mathbf{k},\mathbf{q})]d\mathbf{p}\ d\mathbf{q}-Q_3(\mathbf{k},\mathbf{p})-Q_3(\mathbf{p},\mathbf{k}).\end{aligned} \tag{23}$$

The integral term is the conservative transfer term discussed in detail elsewhere (e.g., Ref. 28). The final two terms are the source terms for scalar fluctuations that arise from the presence of the mean gradient. Equation (23) can be further reduced by introducing the relationships shown in Eqs. (13)

TABLE I. Table of coefficients for $Q(k)$. ''Formula'' refers to $[1/(1-\mu^2)](pq/k)[1/(2\pi)^3]\int_0^{2\pi}\langle\text{Integrand}\rangle d\phi_q$. Here x, y, and z refer to the cosines of angles between the vectors of the triad [see Eqs. (11g)–11(i)], and N^2 is given by $N^2 \equiv \frac{1}{4}(k+p+q)(k+p-q)(k-p+q)(-k+p+q)$.

Name	Integrand	Expanded integrand	Formula
H_1	$k_n P_{j3}(\mathbf{k}) D_{3jn}^{qkp}$	$k_n P_{j3}(\mathbf{k}) P_{3ab}(\mathbf{q}) P_{aj}(\mathbf{k}) P_{bn}(\mathbf{p})$	$\frac{N^2}{8\pi^2}\frac{pq}{k}\left(-\frac{(1+y^2)}{p^2}+\frac{xy}{kp}\right)$
H_2	$k_n P_{j3}(\mathbf{k}) D_{nj3}^{pkq}$	$k_n P_{j3}(\mathbf{k}) P_{nab}(\mathbf{p}) P_{aj}(\mathbf{k}) P_{b3}(\mathbf{q})$	$\frac{N^2}{8\pi^2}\frac{pq}{k}\left(\frac{yz}{pq}-\frac{xy}{kp}\right)$
H_3	$k_n P_{j3}(\mathbf{k}) D_{j3n}^{kqp}$	$k_n P_{j3}(\mathbf{k}) P_{jab}(\mathbf{k}) P_{a3}(\mathbf{q}) P_{bn}(\mathbf{p})$	$\frac{N^2}{8\pi^2}\frac{pq}{k}\left(\frac{(1+y^2)}{p^2}-\frac{yz}{pq}\right)$
H_4	$k_n P_{j3}(\mathbf{k}) C_{nj}^{qpk}$	$k_n P_{j3}(\mathbf{k}) q_a P_{na}(\mathbf{p}) P_{j3}(\mathbf{k})$	$\frac{N^2 q}{4\pi^2 pk}$
H_5	$k_n P_{j3}(\mathbf{k}) D_{n3j}^{pqk}$	$k_n P_{j3}(\mathbf{k}) P_{nab}(\mathbf{p}) P_{a3}(\mathbf{q}) P_{bj}(\mathbf{k})$	$\frac{N^2}{8\pi^2}\frac{pq}{k}\left(\frac{yz}{pq}-\frac{xy}{kp}\right)$
H_6	$k_n P_{j3}(\mathbf{k}) D_{jn3}^{kpq}$	$k_n P_{j3}(\mathbf{k}) P_{jab}(\mathbf{k}) P_{an}(\mathbf{p}) P_{b3}(\mathbf{q})$	$\frac{N^2}{8\pi^2}\frac{pq}{k}\left(\frac{(1+y^2)}{p^2}-\frac{yz}{pq}\right)$
H_7	$k_n P_{j3}(\mathbf{k}) C_{jn}^{qkp}$	$k_n P_{j3}(\mathbf{k}) q_a P_{ja}(\mathbf{k}) P_{n3}(\mathbf{p})$	$\frac{N^2 qz}{8\pi^2 k^2}$
J_1	$P_{3jn}(\mathbf{k}) D_{j3n}^{qkp}$	$P_{3jn}(\mathbf{k}) P_{jab}(\mathbf{q}) P_{a3}(\mathbf{k}) P_{bn}(\mathbf{p})$	$\frac{N^2}{8\pi^2}\frac{pq}{k}\left(-\frac{(1+y^2)}{p^2}+\frac{xy}{kp}-\frac{xz}{kq}+\frac{yz}{pq}\right)$
J_2	$P_{3jn}(\mathbf{k}) D_{nj3}^{pqk}$	$P_{3jn}(\mathbf{k}) P_{nab}(\mathbf{p}) P_{aj}(\mathbf{q}) P_{b3}(\mathbf{k})$	$\frac{N^2}{8\pi^2}\frac{pq}{k}\left(-\frac{(1+z^2)}{q^2}-\frac{xy}{kp}+\frac{xz}{kq}+\frac{yz}{pq}\right)$
J_3	$P_{3jn}(\mathbf{k}) D_{3jn}^{kqp}$	$P_{3jn}(\mathbf{k}) P_{3ab}(\mathbf{k}) P_{aj}(\mathbf{q}) P_{bn}(\mathbf{p})$	$\frac{N^2}{8\pi^2}\frac{pq}{k}\left(\frac{(1+y^2)}{p^2}+\frac{(1+z^2)}{q^2}-2\frac{yz}{pq}\right)$
J_4	$P_{3jn}(\mathbf{k}) D_{n3j}^{pkq}$	$P_{3jn}(\mathbf{k}) P_{nab}(\mathbf{p}) P_{a3}(\mathbf{k}) P_{bj}(\mathbf{q})$	$\frac{N^2}{8\pi^2}\frac{pq}{k}\left(-\frac{(1+z^2)}{q^2}-\frac{xy}{kp}+\frac{xz}{kq}+\frac{yz}{pq}\right)$
J_5	$P_{3jn}(\mathbf{k}) C_{nj}^{kpq}$	$P_{3jn}(\mathbf{k}) k_a P_{na}(\mathbf{p}) P_{j3}(\mathbf{q})$	$\frac{N^2}{8\pi^2}\frac{pq}{k}\left(\frac{(1+y^2)}{p^2}-\frac{yz}{pq}\right)$
J_6	$P_{3jn}(\mathbf{k}) C_{jn}^{kqp}$	$P_{3jn}(\mathbf{k}) k_a P_{ja}(\mathbf{q}) P_{n3}(\mathbf{p})$	$\frac{N^2}{8\pi^2}\frac{pq}{k}\left(\frac{(1+z^2)}{q^2}-\frac{yz}{pq}\right)$
J_7	$P_{3jn}(\mathbf{k}) D_{jn3}^{qpk}$	$P_{3jn}(\mathbf{k}) P_{jab}(\mathbf{q}) P_{an}(\mathbf{p}) P_{b3}(\mathbf{k})$	$\frac{N^2}{8\pi^2}\frac{pq}{k}\left(-\frac{(1+y^2)}{p^2}+\frac{xy}{kp}-\frac{xz}{kq}+\frac{yz}{pq}\right)$

and (20), eliminating the common factor $\hat{\delta}(\mathbf{k}+\mathbf{p})$, and taking advantage of the fact that $M_n(-\mathbf{p},-\mathbf{k},-\mathbf{q})=-M_n(\mathbf{p},\mathbf{k},\mathbf{q})$ and $P_{33}(\mathbf{k})=1-\mu^2$, yielding

$$\left(\frac{\partial}{\partial t}+2\,\mathrm{Pe}^{-1}k^2\right)B(k,\mu)=\int\int ik_n M_n(\mathbf{p},\mathbf{k},\mathbf{q})\,d\mathbf{p}\,d\mathbf{q} - Q(k)(1-\mu^2). \tag{24}$$

B. EDQNM closure and final equations for $B(k,\mu)$

A rigorous application of EDQNM theory yields the following expression for the triple correlation (see Appendix A for details):

$$\begin{aligned}M_n(\mathbf{p},\mathbf{k},\mathbf{q}) = -i\hat{\delta}(\mathbf{k}+\mathbf{p}+\mathbf{q})\big(&-\Theta_{M'}^{pkq;pkq}\{-\Theta_R^{pqk}[D_{3n3}^{qpk}R(k)R(p)+D_{n33}^{pqk}R(k)R(q)+D_{3n3}^{kpq}R(p)R(q)]+C_{n3}^{qpk}R(p)Q(k)\\&+C_{3n}^{qkp}R(k)Q(p)+D_{n33}^{pkq}R(k)Q(q)+D_{33n}^{kqp}R(p)Q(q)\}-\Theta_{M'}^{pkq;pqk}\{-\Theta_R^{pkq}[D_{3n3}^{qpk}R(k)R(p)+D_{n33}^{pkq}R(k)R(q)\\&+D_{3n3}^{kpq}R(p)R(q)]+D_{33n}^{qkp}R(p)Q(k)+D_{n33}^{pqk}R(q)Q(k)+C_{3n}^{kqp}R(q)Q(p)+C_{n3}^{kpq}R(p)Q(q)\}\\&+\Theta_M^{pkq}[C_{3n}^{qkp}Q(k)Q(p)+D_{n33}^{pkq}Q(k)Q(q)+C_{3n}^{kqp}Q(p)Q(q)+A_n^{qp}R(p)B(k,\mu)+A_n^{kp}R(p)B(q,\mu'')]\big),\end{aligned} \tag{25a}$$

where the definitions for C_{ij}^{kpq} and D_{ijm}^{kpq} given in Eqs. (17b) and (17c) still apply, and

$$A_i^{kp}=A_i(\mathbf{k},\mathbf{p})=2k_n P_{in}(\mathbf{p}), \tag{25b}$$

$$\Theta_M^{kpq}=\frac{1-e^{-\mu_M^{kpq}t}}{\mu_M^{kpq}}, \tag{25c}$$

$$\Theta_{M'}^{kpq;k'p'q'}=\begin{cases}\dfrac{1}{\mu_T^{k'p'q'}}\left[\dfrac{(1-e^{-\mu_M^{kpq}t})}{\mu_M^{kpq}}+\dfrac{(e^{-\mu_M^{kpq}t}-e^{-\mu_T^{k'p'q'}t})}{(\mu_M^{kpq}-\mu_T^{k'p'q'})}\right], & \mu_M^{kpq}\neq\mu_T^{k'p'q'},\\ \dfrac{1}{\mu_T^{k'p'q'}}\left[\dfrac{(1-e^{-\mu_M^{kpq}t})}{\mu_M^{kpq}}-te^{-\mu_M^{kpq}t}\right], & \mu_M^{kpq}=\mu_T^{k'p'q'},\end{cases} \tag{25d}$$

$$\mu_M^{kpq}=c_4\mu_k+c_5(\mu_p+\mu_q)+R_L^{-1}k^2+\mathrm{Pe}^{-1}(p^2+q^2). \tag{25e}$$

The coefficients c_4 and c_5 are empirical constants associated with scalar transfer. Following the analysis of Andre and Lesieur,[29] the coefficients are assigned the value 0.36. This ensures mathematical consistency of the proposed model with earlier isotropic scalar models, in the limit of a vanishingly small scalar gradient.

The expression for $M_n(\mathbf{p},\mathbf{k},\mathbf{q})$ [Eq. (25a)] can be substituted into Eq. (24) to yield a closed expression for $B(k,\mu)$. However, a complication with $B(k,\mu)$ is its unknown dependency on the angle μ. One method of explicitly representing this dependency is to expand $B(k,\mu)$ in a Legendre polynomial series in μ, as shown below,[25]

$$B(k,\mu)=\sum_{j=0}^{\infty}B_{2j}(k)P_{2j}(\mu). \tag{26}$$

[Because $B(k,\mu)$ is an even function of μ only the even members of the series are nonzero.] Fortunately, in the present application, the infinite series can be truncated after the second term because the higher-order terms have no source, and therefore if they are zero initially they will remain zero for all time. Thus, the angle dependence of the scalar autocorrelation reduces to

$$B(k,\mu)=B_0(k)P_0(\mu)+B_2(k)P_2(\mu), \tag{27}$$

where $P_0(\mu)=1$ and $P_2(\mu)=(3\mu^2-1)/2$.

Upon substituting Eq. (25a) into Eq. (24), re-expressing the nonlinear integral term as shown in Appendix B, and expanding the scalar functions $B(k,\mu)$ and $B(q,\mu'')$ in terms of the Legendre Polynomials [Eq. (27)], a closed form expression for the autocorrelation is obtained. Separate expressions for the spectral coefficients $B_0(k)$ and $B_2(k)$ are then obtained by multiplying the equation by $P_l(\mu)$ ($l=0$ or 2) and integrating with respect to μ, thereby taking advantage of the orthogonal properties of Legendre polynomials,

$$\int_{-1}^{1}P_j(\mu)P_l(\mu)d\mu=\frac{2}{(2l+1)}\,\delta_{jl}. \tag{28}$$

The final expression is (see Herr[30] for details)

$$\begin{aligned}\left(\frac{\partial}{\partial t}+2\,\mathrm{Pe}^{-1}\,k^2\right)B_l(k)=\int_{\Delta}\int(&-\Theta_{M'}^{pkq;pkq}\{-\Theta_R^{pqk}[F_1^lR(k)R(p)+F_2^lR(k)R(q)+F_3^lR(p)R(q)]+F_4^lR(p)Q(k)\\&+F_5^lR(k)Q(p)+F_6^lR(k)Q(q)+F_7^lR(p)Q(q)\}-\Theta_{M'}^{pkq;pqk}\{-\Theta_R^{pkq}[G_1^lR(k)R(p)\\&+G_2^lR(k)R(q)+G_3^lR(p)R(q)]+G_4^lR(p)Q(k)+G_5^lR(q)Q(k)+G_6^lR(q)Q(p)\\&+G_7^lR(p)Q(q)\}+\Theta_M^{pkq}[M_1^lQ(k)Q(p)+M_2^lQ(k)Q(q)+M_3^lQ(p)Q(q)+M_4^lR(p)B_l(k)\\&+M_5^lR(p)B_l(q)])dp\;dq-\tfrac{2}{3}(1-l)Q(k),\end{aligned} \tag{29}$$

where ''l'' refers to the index of the Legendre polynomial (0 or 2). The 19 geometric cofactors that result from the angle integrations F_1^l–F_7^l, G_1^l–G_7^l, and M_1^l–M_5^l are summarized in Table II.

VI. NUMERICAL PROCEDURE

The dynamic equations for $R(k)$, $Q(k)$, $B_0(k)$, and $B_2(k)$ [Eqs. (11a), (18), and (29), respectively] are classified as integrodifferential equations, and therefore updating them requires a numerical procedure for evaluating the convolution integral at each time step. Homogeneity requires that the integral be evaluated over values of p and q that form a closed triad. This region of the p-q space is shown schematically in Fig. 1 for $k=2$. The integral was evaluated using a trapezoid rule in two dimensions. Each point was weighted by either unity, $\frac{1}{2}$, or $\frac{1}{4}$ depending on whether the point was in the center of the domain of integration, on a bounding line, or a bounding corner (see Fig. 1). It would be possible to improve the accuracy of the numerical integration by substituting a higher-order approximation for the integrand (e.g., Simpson's rule), however, a word of caution is required. Some of the quantities transported by the nonlinear terms should be conserved under the action of the integral. Nonuniform weighting of the internal points may compromise the conservation principle, because cancellations required for

TABLE II. Table of coefficients in the equation for $B_l(k)$, where l refers to the order of the Legendre series (0 or 2). ''Formula'' refers to: $[(l+\frac{1}{2})/(2\pi)^3](pq/k)\int_{-1}^{1}\int_{0}^{2\pi}\langle\text{Integrand}\rangle P_l(\mu)d\phi_q\, d\mu$. Here x, y, and z refer to the cosines of angles between the vectors of the triad [see Eqs. (11g)–(11i)], and N^2 is given by $N^2 \equiv \frac{1}{4}(k+p+q)(k+p-q)(k-p+q)(-k+p+q)$.

Name	Integrand	Integrand (expanded)	Formula
F_1^l	$k_i D_{3i3}^{qpk}$	$k_i P_{3ab}(\mathbf{q}) P_{ai}(\mathbf{p}) P_{b3}(\mathbf{k})$	$\frac{N^2}{12\pi^2}\frac{pq}{k}(1-l)\left(-\frac{(1+y^2)}{p^2}+\frac{xy}{kp}\right)$
F_2^l	$k_i D_{i33}^{pqk}$	$k_i P_{iab}(\mathbf{p}) P_{a3}(\mathbf{q}) P_{b3}(\mathbf{k})$	$\frac{N^2}{12\pi^2}\frac{pq}{k}(1-l)\left(\frac{(yz)}{pq}-\frac{xy}{kp}\right)$
F_3^l	$k_i D_{3i3}^{kpq}$	$k_i P_{3ab}(\mathbf{k}) P_{ai}(\mathbf{p}) P_{b3}(\mathbf{q})$	$\frac{N^2}{12\pi^2}\frac{pq}{k}(1-l)\left(\frac{(1+y^2)}{p^2}-\frac{yz}{pq}\right)$
F_4^l	$k_i C_{i3}^{qpk}$	$k_i q_a P_{ia}(\mathbf{p}) P_{33}(\mathbf{k})$	$-\frac{N^2(1-l)q}{6\pi^2 pk}$
F_5^l	$k_i C_{3i}^{qkp}$	$k_i q_a P_{3a}(\mathbf{k}) P_{i3}(\mathbf{p})$	$\frac{N^2}{12\pi^2}\frac{pq}{k}(1-l)\frac{z}{kp}$
F_6^l	$k_i D_{i33}^{pkq}$	$k_i P_{iab}(\mathbf{p}) P_{a3}(\mathbf{k}) P_{b3}(\mathbf{q})$	$\frac{N^2}{12\pi^2}\frac{pq}{k}(1-l)\left(\frac{yz}{pq}-\frac{xy}{kp}\right)$
F_7^l	$k_i D_{33i}^{kqp}$	$k_i P_{3ab}(\mathbf{k}) P_{a3}(\mathbf{q}) P_{bi}(\mathbf{p})$	$\frac{N^2}{12\pi^2}\frac{pq}{k}(1-l)\left(\frac{(1+y^2)}{p^2}-\frac{yz}{pq}\right)$
G_1^l	$k_i D_{3i3}^{qpk}$	$k_i P_{3ab}(\mathbf{q}) P_{ai}(\mathbf{p}) P_{b3}(\mathbf{k})$	$\frac{N^2}{12\pi^2}\frac{pq}{k}(1-l)\left(-\frac{(1+y^2)}{p^2}+\frac{xy}{kp}\right)$
G_2^l	$k_i D_{i33}^{pkq}$	$k_i P_{iab}(\mathbf{p}) P_{a3}(\mathbf{k}) P_{b3}(\mathbf{q})$	$\frac{N^2}{12\pi^2}\frac{pq}{k}(1-l)\left(\frac{(yz)}{pq}-\frac{xy}{kp}\right)$
G_3^l	$k_i D_{3i3}^{kpq}$	$k_i P_{3ab}(\mathbf{k}) P_{ai}(\mathbf{p}) P_{b3}(\mathbf{q})$	$\frac{N^2}{12\pi^2}\frac{pq}{k}(1-l)\left(\frac{(1+y^2)}{p^2}-\frac{yz}{pq}\right)$
G_4^l	$k_i D_{33i}^{qkp}$	$k_i P_{3ab}(\mathbf{q}) P_{a3}(\mathbf{k}) P_{bi}(\mathbf{p})$	$\frac{N^2}{12\pi^2}\frac{pq}{k}(1-l)\left(-\frac{(1+y^2)}{p^2}+\frac{xy}{kp}\right)$
G_5^l	$k_i D_{i33}^{pqk}$	$k_i P_{iab}(\mathbf{p}) P_{a3}(\mathbf{q}) P_{b3}(\mathbf{k})$	$\frac{N^2}{12\pi^2}\frac{pq}{k}(1-l)\left(\frac{yz}{pq}-\frac{xy}{kp}\right)$
G_6^l	$k_i C_{3i}^{kqp}$	$k_i k_a P_{3a}(\mathbf{q}) P_{i3}(\mathbf{p})$	$\frac{N^2}{12\pi^2}\frac{pq}{k}\left[-(1-l)\frac{yz}{pq}+\left(1+\frac{l}{2}\right)\frac{N^2}{k^2p^2q^2}\right]$
G_7^l	$k_i C_{i3}^{kpq}$	$k_i k_a P_{ia}(\mathbf{p}) P_{33}(\mathbf{q})$	$\frac{N^2}{12\pi^2}\frac{pq}{k}\left[(1-l)\left(\frac{1+y^2}{p^2}\right)+\left(1+\frac{l}{2}\right)\frac{N^2}{k^2p^2q^2}\right]$
M_1^l	$k_i C_{3i}^{qkp}$	$k_i q_a P_{3a}(\mathbf{k}) P_{i3}(\mathbf{p})$	$\frac{N^2}{12\pi^2}\frac{pq}{k}(1-l)\frac{z}{kp}$
M_2^l	$k_i D_{i33}^{pkq}$	$k_i P_{iab}(\mathbf{p}) P_{a3}(\mathbf{k}) P_{b3}(\mathbf{q})$	$\frac{N^2}{12\pi^2}\frac{pq}{k}(1-l)\left(\frac{yz}{pq}-\frac{xy}{kp}\right)$
M_3^l	$k_i C_{3i}^{kqp}$	$k_i k_a P_{3a}(\mathbf{q}) P_{i3}(\mathbf{p})$	$\frac{N^2}{12\pi^2}\frac{pq}{k}\left[-(1-l)\frac{yz}{pq}+\left(1+\frac{l}{2}\right)\frac{N^2}{k^2p^2q^2}\right]$
M_4^l	$k_i A_i^{qp}$	$2k_i q_a P_{ia}(\mathbf{p})$	$-\frac{N^2 q}{2\pi^2 pk}$
M_5^l	$k_i A_i^{kp}$	$2k_i k_a P_{ia}(\mathbf{p})$	$\frac{N^2 q}{4\pi^2 pk}\left[2\left(1-\frac{l}{2}\right)+\frac{l}{2}(3y^2-1)\right]$

conservation may be altered by the different weights. For example, if a particular triad is to appear twice in the integrand, however, it is weighted differently in each case, the system may not precisely conserve the transported quantity. We therefore elected to use a trapezoid rule even though it is less accurate because it ensures uniform weighting of all equivalent points.

VII. DIRECT NUMERICAL SIMULATIONS

Direct numerical simulations of a passive scalar advected by an incompressible fluid were performed on a 128^3 lattice using a standard pseudospectral Galerkin method to update the fluid velocity and scalar transport equations.[31,32] The spectral code was a modified version of that described in Chen and Shan[33] for the velocity field. The simulations for this study were performed on the massively parallel CM-5 at Los Alamos National Laboratory. The basic algorithm is equivalent to the one described in the textbook by Canuto *et al.*[34] The aliasing errors in the pseudospectral simulation were completely eliminated by truncating all modes with wave numbers larger than 47.5 (the two-thirds rule). The physical parameters used in the simulations are summarized in Table III. The fluid viscosity was set to give an average spatial resolution parameter $k_{\max}\,\eta = 1.56$, the temporal resolution parameter or CFL number was 0.23, and the Prandtl number was 0.5, therefore both the velocity and scalar field

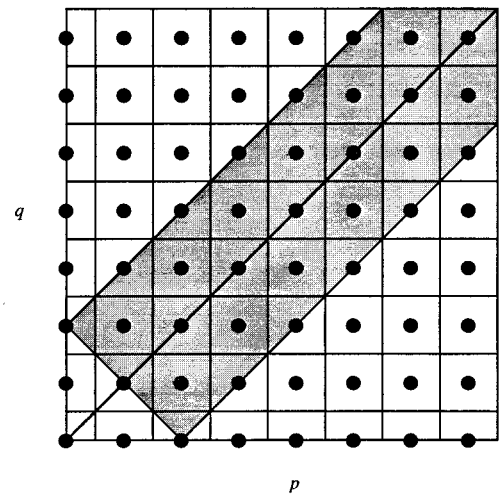

FIG. 1. Schematic of the region of integration for wave number $k=2$. The gray region is the domain of integration. Points in the center of the domain have unity weighting while points on the bounding lines are weighted by $\frac{1}{2}$ and points in the corners by $\frac{1}{4}$.

were well resolved in space and in time in the simulation.[35] The velocity field was made stationary by maintaining constant total energy in each of the first two wave number shells ($0.5 \leqslant k \leqslant 1.5$ and $1.5 \leqslant k \leqslant 2.5$), with the energy ratio between the two shells consistent with $k^{-5/3}$. Since the nodes are not evenly distributed in the spherical shells in wave vector space, a smoothing operation[36] was applied to the energy spectrum $E(k)$. Because the velocity field was stationary, the scalar fluctuations, which were initially set to zero, asymptotically approached a constant mean value at long times that was determined by a balance between the fluctuation source due to the mean gradient and the rate of dissipation controlled by spectral cascade and dissipation.

The direct numerical simulation was first run with the velocity field only for about ten eddy turnover times to obtain a statistically stationary hydrodynamic field. The scalar field was then introduced and the simulation was continued for an additional 60 eddy turnover times. We assumed the scalar field had achieved a statistically stationary state after 30 eddy turnover times, and so the remaining 30 eddy turnover times were used to compute the average values of the scalar and scalar-velocity correlations. One motivation for running the simulations for such long times was to achieve meaningful statistical measures of the mean scalar quantities of interest. Since most of the statistics addressed in the EDQNM analysis are directly related to the large-scale scalar field, and there are a limited number of large-scale modes in the computational domain, it was necessary to carry out the simulation for at least 60 eddy turnover times. To our knowledge, such long-time simulations have been performed in only a few studies (e.g., Ref. 6). Since the focus of this paper is the EDQNM analysis, the direct numerical simulation was used to guide the analysis and provide the necessary information to estimate some of the model parameters (c_2 and c_3). We therefore only report one simulation here. A more detailed comparison between the direct numerical simulations and the EDQNM model, including a parametric study, will be reported in a future publication.

Single-point averages of the scalar autocorrelation and velocity-scalar cross correlation were determined by averaging the values over the calculation grid. Spherically average spectra for the cross- and autocorrelations were determined from sums over shells, as shown below:

$$Q(k_i)=\frac{3\pi^2}{k_i^2}\sum_{\phi=0}^{2\pi}\sum_{\mu=-1}^{1}\frac{1}{2}\left[\hat{u}_3(\mathbf{k})\hat{\Phi}^*(\mathbf{k})+\hat{u}_3^*(\mathbf{k})\hat{\Phi}(\mathbf{k})\right]\Bigg|_{k_i-\Delta k/2\leqslant|\mathbf{k}|\leqslant k_i+\Delta k/2}, \tag{30a}$$

$$B(k_i)=\frac{\pi^2}{k_i^2}\sum_{\phi=0}^{2\pi}\sum_{\mu=-1}^{1}\left[\hat{\Phi}(\mathbf{k})\hat{\Phi}^*(\mathbf{k})\right]\Bigg|_{k_i-\Delta k/2\leqslant|\mathbf{k}|\leqslant k_i+\Delta k/2}. \tag{30b}$$

The angle-dependent spectra for the autocorrelation were then determined using a conical average, defined by

$$B(k_i,\mu_i)=\frac{\pi^2}{k_i^2}\sum_{\phi=0}^{2\pi}\left[\hat{\Phi}(\mathbf{k})\hat{\Phi}^*(\mathbf{k})\right]\Bigg|_{\substack{k_i-\frac{\Delta k}{2}\leqslant|\mathbf{k}|\leqslant k_i+\frac{\Delta k}{2}\\ \mu_i-\frac{\Delta\mu}{2}\leqslant\mu\leqslant\mu_i+\frac{\Delta\mu}{2}}}. \tag{30c}$$

VIII. RESULTS AND DISCUSSION

As mentioned previously, the model contains two adjustable constants (c_2 and c_3) that arise from the eddy damping terms in the cross-correlation spectrum. The constants cannot be constrained by imposing an asymptotic form for the cross-correlation spectrum at high Reynolds numbers since none exists. Instead, we have elected to fix the constants by fitting the Q spectrum at long times to the time-average spectrum from the numerical simulations. The figure of merit for the optimization is the mean value of the single-point correlation

TABLE III. Parameter values used in direct numerical simulations and model calculations. Dimensional parameters are based on arbitrary units. Here $U_{\rm rms}$ refers to the turbulence intensity; ϵ is the dissipation rate; ν is the kinematic viscosity; L is the integral scale; λ is the Taylor Microscale; η is the Kolmogorov scale; T_e is the large eddy turnover time; Γ is the magnitude of the mean scalar gradient; and $\sqrt{\overline{\Phi'^2}}$ is the root mean square of the scalar fluctuations. As for the dimensionless parameters, R_L and R_λ are Reynolds numbers based on the integral scale and Taylor microscale, respectively; P is the Prandtl number; and $\Phi_{\rm rms}$ is the *dimensionless* root mean square scalar fluctuation (based on the characteristic scalar value ΓL).

	Dimensional parameters (arbitrary units)									Dimensionless parameters			
Title	$U_{\rm rms}$	ϵ	ν	L	λ	η	T_e	Γ	$\sqrt{\overline{\Phi'^2}}$	R_L	R_λ	P	$\Phi_{\rm rms}$
DNS	0.84	0.19	0.006	1.59	0.58	0.033	1.9	1.0	2.15	223	81	0.5	1.35
EDQNM	0.88	0.19	0.006	1.59	0.61	0.033	1.8	1.0	2.23	233	89	0.5	1.40

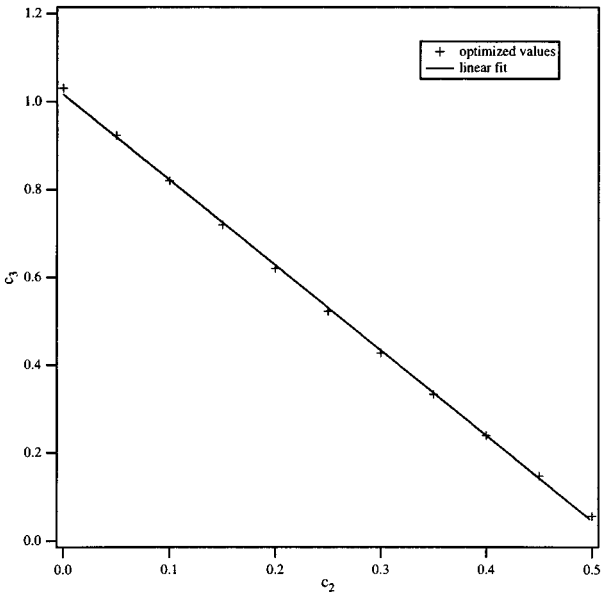

FIG. 2. Optimal values of the coefficients c_2 and c_3 in the eddy damping terms associated with $T_{jn}(\mathbf{k},\mathbf{p},\mathbf{q})$. The coefficients were determined by fitting the $Q(k)$ spectrum from the model to the equivalent spectrum from the direct numerical simulations. The results shown in the paper are based on the combination (0, 1.03).

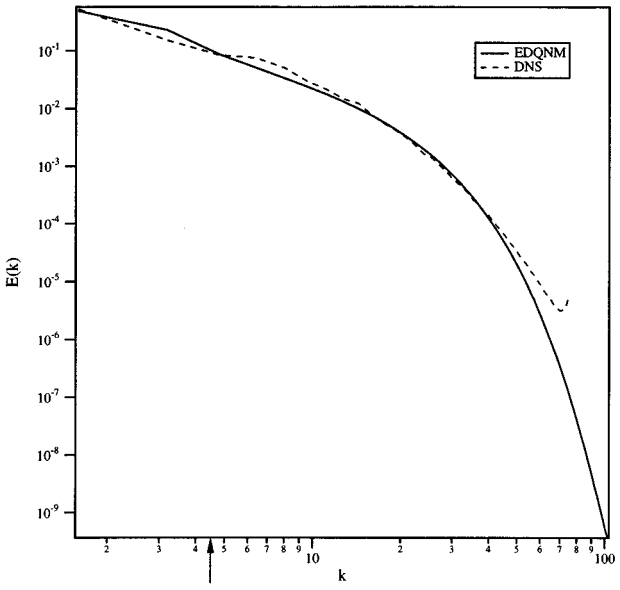

FIG. 3. The turbulent energy spectrum for the model (solid line) and simulation (dashed line). The spectrum from the simulation was averaged over 30 eddy turnover times.

$\overline{u_3\Phi'}$. Figure 2 shows the acceptable pairs of values of c_2 and c_3. The solid line is a least squares fit of the results. It is interesting to note that the relationship between the two coefficients is linear, which is consistent with the other pair of coefficients in the autocorrelation spectrum (i.e., c_4 and c_5).[28] We chose the combination c_2, c_3=(0,1.03) for the calculations shown in this paper, however, the results were relatively insensitive to the particular combination used.

A. Energy

Much of the earlier work with the EDQNM model has focused on decaying isotropic or axisymmetric turbulence. The numerical simulations in the present study are made stationary by forcing the low wave number end of the spectrum, therefore the EDQNM model for the energy must include forcing terms as well to be consistent. A forcing function was added to the standard EDQNM model to supply a constant (in time) source of energy to the first two wave numbers [see Eq. (11a), and related equations in the text]. At steady state, the rate of energy addition to the fluid must equal the rate of viscous dissipation (ϵ), hence

$$\epsilon = \frac{1}{2\pi^2}(F_1 + 4F_2), \tag{31}$$

where F_k is the magnitude of forcing at wave number k. The dissipation rate in the simulations can be readily determined from the energy spectrum. Equation (31) provides a constraint on the values of F_1 and F_2. A specific combination of F_1 and F_2 satisfying Eq. (31) was chosen so as to match the integral length scale of the numerical simulation as well. Figure 3 shows a comparison between the energy spectrum from the EDQNM model and an average spectrum from the numerical simulations. There is reasonable agreement over most of the wave numbers. The differences are attributed to two causes: (i) the imperfect match of the forcing in the two systems; and (ii) neglecting the contribution of the forcing term to energy transfer in the EDQNM model. The effect of the latter is apparent in the DNS spectrum just beyond the forcing range (indicated with an arrow in Fig. 3); that is, there is a noticeable bump in the energy spectrum at that point. Most likely, this results from an enhancement in the rate of energy transfer to the wave number just beyond the forcing band due to the forcing. This is not accounted for in the EDQNM model. To compensate, the model must overpredict the energy at the second wave number so as to yield an integral scale in agreement with the simulations. Additional work is required to correctly incorporate the effect of forcing on the transfer function in the EDQNM equation for the energy. However, despite these objections, we believe there is sufficient agreement between the predicted energy spectrum and the simulations to achieve meaningful comparisons of the other scalar spectra.

B. Single-point scalar statistics

Figure 4(a) illustrates the time dependence of the scalar-velocity cross correlation (turbulent scalar flux). The DNS results are spatial averages over the domain of integration (cube of length 2π) and the EDQNM model results were determined from Eq. (14). As noted above, the scalar statistics are particularly troublesome, requiring several eddy turnover times to achieve reasonable statistical convergence. Nevertheless, there appears to be quantitative agreement between the model and simulation results. It should be noted that the coefficients c_2 and c_3 were chosen to optimize the agreement at long times, so the test is whether the model

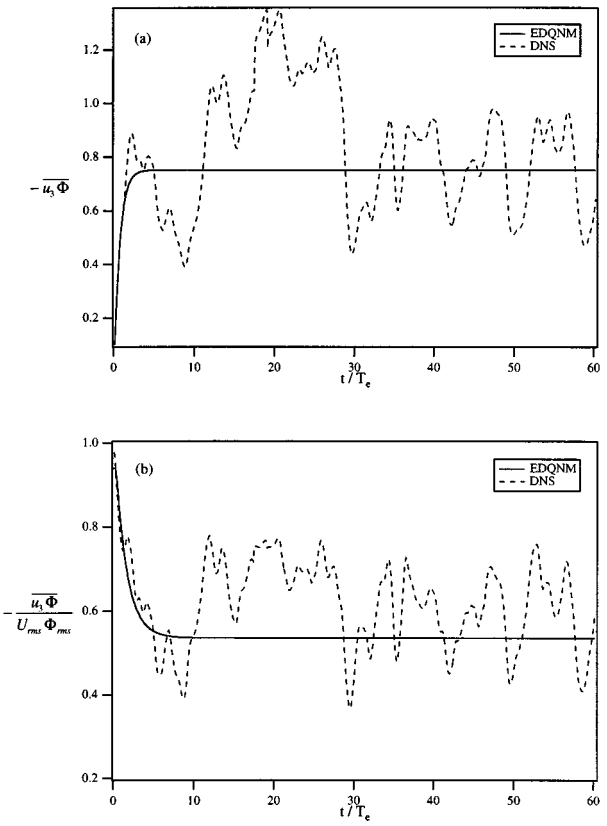

FIG. 4. (a) Single-point scalar-velocity correlation as a function of time. The solid curve was determined from the model and the dashed curve from the numerical simulation. Simulation values are instantaneous volume averages of the correlation. (b) The same correlation normalized by the product turbulence intensity $U_{\rm rms}$ times the root mean square scalar fluctuation $\Phi_{\rm rms}$. The correlation is initially very high (i.e., near unity), however, it diminishes in time due to transfer processes that tend to decorrelate the scalar and velocity fields.

captures the transient behavior. It appears to do well. Figure 4(b) shows the cross correlation normalized by the local (in time) value of $U_{\rm rms}\Phi_{\rm rms}$. The Schwartz inequality restricts this normalized correlation to be less than unity. Both the DNS and model predict that at early times, the correlation is nearly unity (i.e., the velocity and scalar fluctuations are strongly correlated), but at later times the correlation is diminished, ultimately approaching $\sim$0.6 as time approaches infinity. The strong correlation at early times results from the dominance of the source terms in the scalar transport equations that produce scalar fluctuations that are precisely correlated to the eddy motion. At later times, this strong correlation is diminished by the different rates of spectral transfer of energy and scalar concentration that results from differences in the convective terms for each quantity. A modal analysis developed by Brasseur and Wei[37] was used to qualitatively confirm this result. In addition, the DNS results appear to corroborate the model prediction of the *rate* of decorrelation of these two fields.

Here $\Phi_{\rm rms}$ was determined from the simulations again by taking a volume average and from the EDQNM model by evaluating Eq. (21). The results are summarized in Fig. 5. This comparison is perhaps a more direct evaluation of the model since there are no adjustable parameters in the equation for $B_0(k)$ (aside from those fixed in earlier studies). The spatially averaged scalar autocorrelation fluctuates slowly with a period of several eddy turnover times. A comparison between the simulation and EDQNM model results shows that the time-average value of the scalar autocorrelation is predicted to within 4% of the simulation value.

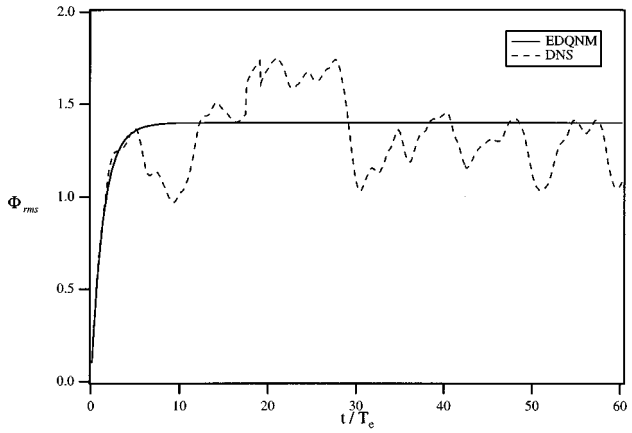

FIG. 5. Single-point scalar autocorrelation as a function of time. The solid curve was determined from the model and the dashed curve from the numerical simulation. Simulation values are instantaneous volume averages of the correlation.

Several earlier studies of passive scalars in the presence of a uniform mean gradient have focused on the magnitude of derivatives in the direction of the mean gradient and in the transverse direction.[2,6] Scalar derivatives differ from the previous statistics in that they explicitly involve the angle dependence of the scalar autocorrelation. That is readily apparent from the definitions for the gradients shown below:

$$\overline{\left(\frac{\partial\Phi}{\partial x_3}\right)^2}=\frac{1}{2\pi^2}\left(\frac{2}{3}\int_0^\infty B_0(k)k^4\,dk+\frac{4}{15}\int_0^\infty B_2(k)k^4\,dk\right), \tag{32a}$$

$$\overline{\left(\frac{\partial\Phi}{\partial x_1}\right)^2}=\overline{\left(\frac{\partial\Phi}{\partial x_2}\right)^2}=\frac{1}{2\pi^2}\left(\frac{2}{3}\int_0^\infty B_0(k)k^4\,dk-\frac{2}{15}\int_0^\infty B_2(k)k^4dk\right). \tag{32b}$$

Figure 6(a) shows a comparison of the square of the gradient in the longitudinal and transverse directions with the EDQNM model result. Again there is reasonable agreement between the model and simulation. The literature often considers the ratio of these two derivatives as a measure of the anisotropy of the scalar field. By definition, this ratio in the model is given by

$$\Lambda=\overline{\left(\frac{\partial\Phi}{\partial x_3}\right)^2}\Bigg/\overline{\left(\frac{\partial\Phi}{\partial x_1}\right)^2}=\frac{1+2A}{1-A}, \tag{33a}$$

where

$$A\equiv\frac{1}{5}\frac{\int_0^\infty B_2(k)k^4\,dk}{\int_0^\infty B_0(k)k^4\,dk}. \tag{33b}$$

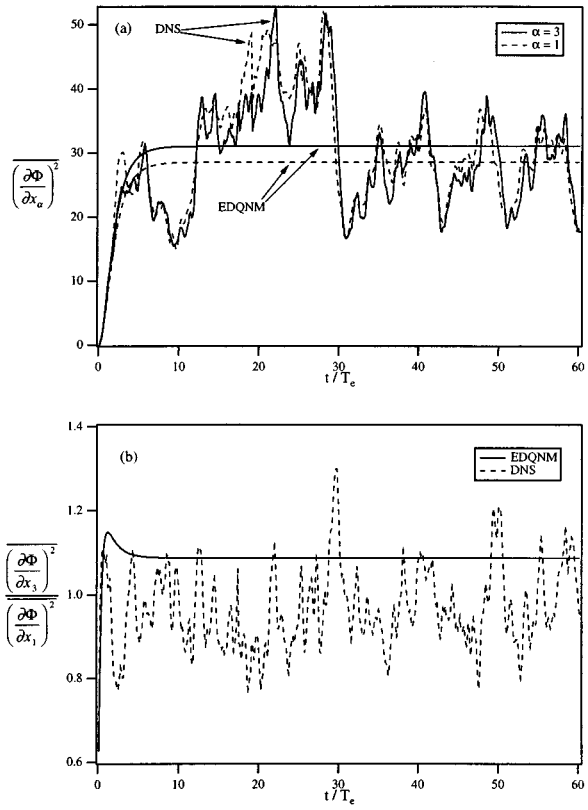

FIG. 6. (a) Average, single-point derivatives of the scalar in the direction of the mean gradient ($[\partial\Phi/\partial x_3]^2$) and in the transverse direction ($[\partial\Phi/\partial x_1]^2$). The subscript α designates the '1' or '3' direction and therefore does *not* imply a summation. (b) Ratio of the two square derivatives as a function of time. Notice that both the model and simulation show this value to be below unity at short times and greater than unity at long times. This is associated with an angular redistribution of the scalar autocorrelation (see Sec. VIII D).

Figure 6(b) is a plot of the predicted and observed ratio of the square of the gradients. It is interesting to note that at short times this ratio is less than unity, and grows above unity at long times. From Eq. (33a) it is apparent that as the ratio increases from a fraction of unity to greater than unity, the variable A must change sign (from negative to positive). Since $B_0(k)$ is positive definite, this implies that $B_2(k)$ must change sign. Indeed, that is what the EDQNM model predicts. At long times, there is some discrepancy between the ratio, Λ, predicted by the EDQNM model ($\Lambda=1.08$) and the value found in the direct numerical simulations ($\Lambda=1.02$). In fact, the anisotropy in the DNS scalar concentration field was barely discernible, especially given the significant statistical fluctuations in the DNS. Interestingly, the model prediction is in closer agreement with earlier experimental measurements by Tong and Warhaft,[2] who found $\Lambda=1.4$ (independent of Reynolds number), and the direct numerical simulations of Pumir,[6] who found values of Λ ranging from 1.07 to 1.33. It should be noted that we found this ratio to be somewhat sensitive to the Reynolds number and very sensitive to the Prandtl number. Furthermore, no effort was made in this study to match the conditions of Tong and Warhaft[2] or Pumir.[6] We will return to the topic of anisotropy as it relates

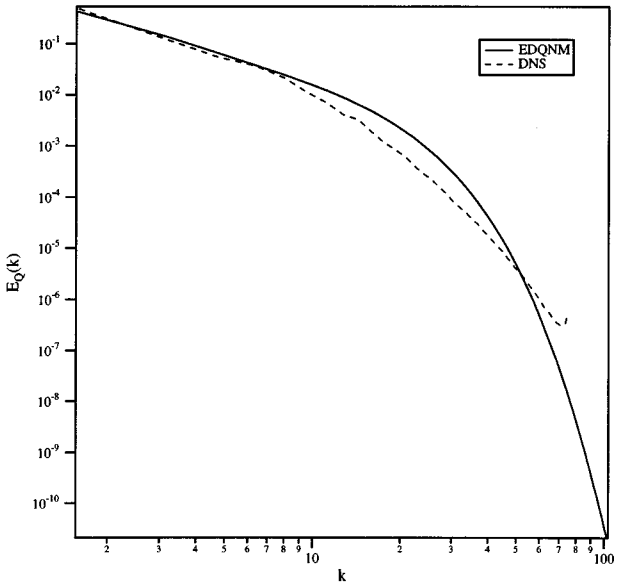

FIG. 7. The scalar-velocity cross-correlation spectrum as a function of wave number. The spectrum is defined as $E_Q(k)=-k^2Q(k)/3\pi^2$. The solid line is the result from the model and the dashed line is the result from the simulation after averaging over 30 eddy turnover times.

to the autocorrelation spectrum in Sec. III C, and again in Sec. III D, which is a more complete discussion of the origins of anisotropy in the EDQNM model.

C. Scalar spectra

The velocity-scalar cross-correlation spectrum, $E_Q(k)\equiv -Q(k)k^2/3\pi^2$, is shown as a function of wave number in Fig. 7. The spectrum is defined such that the integral yields the single-point cross correlation (i.e., $\overline{u_3\Phi'}$). The average cross-correlation spectrum was obtained from the numerical simulations by averaging 30 spectra, each separated by an eddy turnover time. Good agreement is found between the simulation and model results. Furthermore, although the coefficients c_2 and c_3 were chosen to optimize the fit between the simulated and modeled cross correlations, the coefficients predominantly control the lowest wave numbers and have little effect beyond a wave number of approximately 3. Therefore much of the agreement can be attributed to the performance of the EDQNM model and not to the fitting of the coefficients. The equivalent spectrum for the scalar autocorrelation is, by definition, $E_B(k)\equiv B_0(k)k^2/\pi^2$. Figure 8 shows a comparison of this spectrum with the simulation. The model again does very well in predicting the correct scalar spectrum, except at the highest wave numbers.

A critical feature of the passive scalar in the presence of a mean gradient is the reduction in symmetry from isotropic (no mean gradient) to axisymmetric. This reduction in symmetry is responsible for the discrepancy in the magnitude of the derivatives of the scalar in the direction parallel and perpendicular to the mean gradient. The anisotropy in the scalar autocorrelation can be observed directly in the simulations by substituting conical averages [Eq. (30c)] for the shell av-

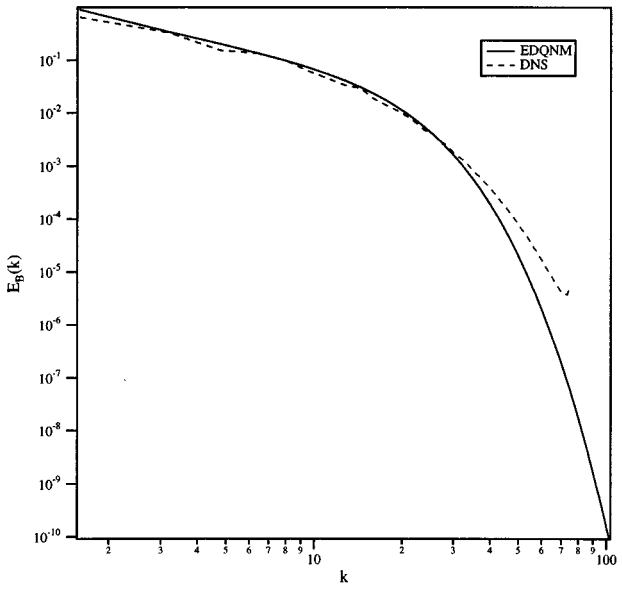

FIG. 8. The scalar autocorrelation spectrum as a function of wave number. The spectrum is defined as $E_B(k)=k^2B_0(k)/\pi^2$. The solid line is the result from the model and the dashed line is the result from the simulation after averaging over 30 eddy turnover times.

erages used in an isotropic system [Eq. (30b)]. Unfortunately, statistical noise due to insufficient grid resolution in the simulations makes it difficult to observe the angle dependence directly, however, we can calculate the spectrum integrated over ranges of the angle μ so that we may look for systematic deviations from the isotropic case. For example, Fig. 9 illustrates the scalar autocorrelation integrated over ranges of μ defined by $0\leqslant\mu\leqslant\frac{1}{2}$ and $\frac{1}{2}\leqslant\mu\leqslant1$. The individual points are the numerical simulations and the solid lines are determined from the analytical formulas shown below:

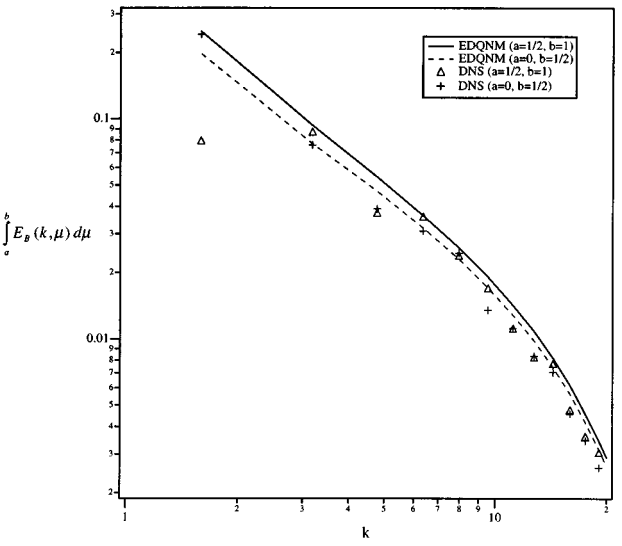

FIG. 9. Partially integrated scalar autocorrelation spectra from the EDQNM model (solid and dashed lines) and numerical simulations (symbols). The coefficients (a,b) are either $(0,\ \frac{1}{2})$ or $(\frac{1}{2},1)$. Notice that the model predicts that the latter integrated spectrum exceeds the former integrated spectrum at long times. A similar result is observed in most of the DNS points as well.

$$\int_0^{1/2} E_B(k,\mu)\,d\mu=\frac{k^2}{2\pi^2}\left(\frac{1}{2}B_0(k)-\frac{3}{16}B_2(k)\right), \tag{34a}$$

$$\int_{1/2}^{1} E_B(k,\mu)\,d\mu=\frac{k^2}{2\pi^2}\left(\frac{1}{2}B_0(k)+\frac{3}{16}B_2(k)\right). \tag{34b}$$

At long times, the EDQNM model predicts that the second integral [Eq. (34b)] exceeds the first integral [Eq. (34a)] at all wave numbers. Likewise, most of the DNS points follow this trend. The major exception occurs at the very first wave number, where the trend in the DNS is strongly reversed. This reversal may be an artifact of the relatively poor grid resolution in the first shell of wave numbers. Nevertheless, despite the scatter in the DNS data, the trends throughout the remainder of the spectrum are represented reasonably accurately by the model. In particular, the model correctly predicts that the largest deviation between the two spectra occurs at low wave numbers, and diminishes thereafter with increasing wave number.

D. Anisotropy in the EDQNM model

Thus far, we have examined the anisotropy in the scalar autocorrelation by evaluating derivatives in the directions parallel and perpendicular to the mean gradient (Fig. 6) and by examining partially integrated spectra (Fig. 9). Now that we have some confidence in the model's ability to predict the scalar correlations, it is insightful to consider the mechanisms responsible for anisotropy in the model. The mechanisms suggest physical explanations for the effects observed in the direct numerical simulations presented here and elsewhere and experiments in the literature.

Anisotropy in the EDQNM model for the scalar autocorrelation is represented entirely by $B_2(k)$; that is, if $B_2(k)=0$, the scalar spectrum is, by definition, isotropic. Recall in the governing equation for $B(k,\mu)$ [Eq. (24)], the anisotropic source term is

$$Q_3(\mathbf{k})=Q(k)P_{33}(\mathbf{k})=Q(k)(1-\mu^2). \tag{35}$$

Thus, $Q_3(\mathbf{k})$ is not only a source of scalar fluctuations, but also a source of anisotropy in the scalar spectrum as well. Upon expanding Eq. (24) in terms of Legendre polynomials, the anisotropy in the source term [Eq. (35)] is manifested in the two separate source terms in the equations governing $B_0(k)$ and $B_2(k)$ that are equal in magnitude but opposite in sign [see Eq. (29)]. This can be illustrated by considering the behavior of Eq. (29) in the limit that the source terms dominate the nonlinear transfer terms and dissipation. In this limit, the coefficients $B_0(k)$ and $B_2(k)$ would be equal in magnitude and opposite in sign [i.e., $B_2(k)=-B_0(k)$], yielding an autocorrelation of the form

$$B(k,\mu)=B_0(k)+B_2(k)(\tfrac{3}{2}\mu^2-\tfrac{1}{2})=\tfrac{3}{2}B_0(k)(1-\mu^2). \tag{36}$$

The source term, therefore, attempts to impose its anisotropy on the scalar spectrum. Furthermore, close examination of Table II shows that most of the coefficients in Eq. (29) associated with nonlinear transfer of the scalar are also consistent with the source term, i.e., they only change sign when l changes from 0 to 2. All coefficients that are proportional to

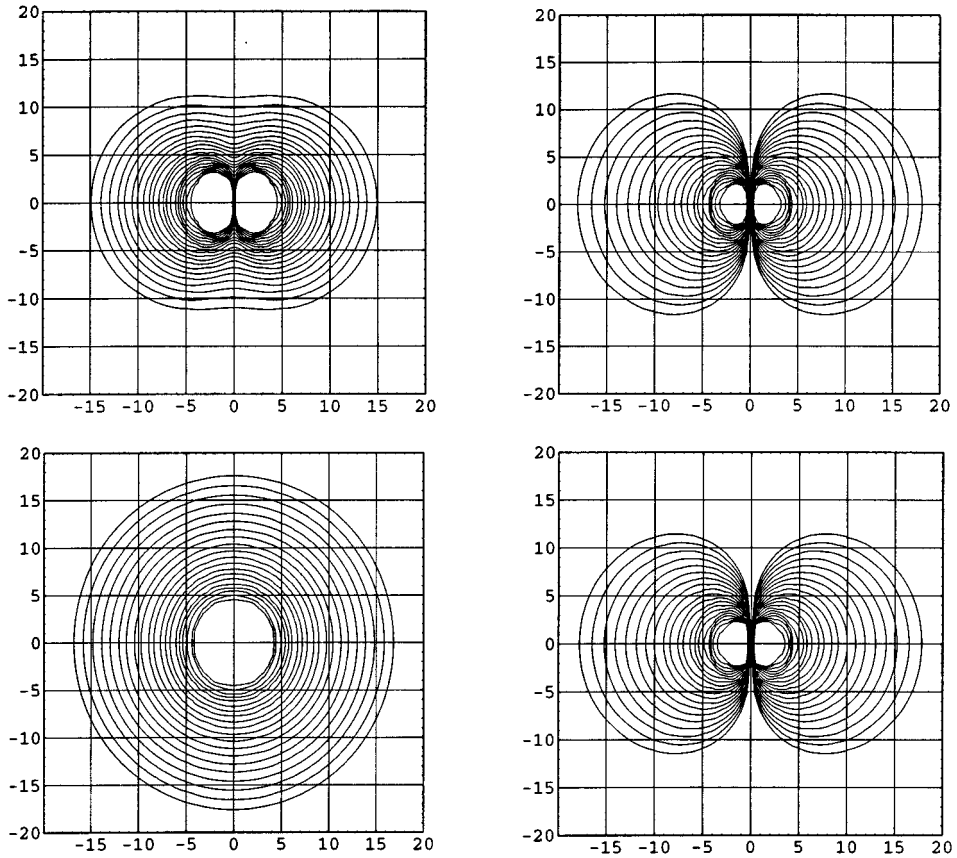

FIG. 10. Two-dimensional contour plots of $B(k,\mu)$ and its source term $Q_3(k,\mu)$ as a function of the wave numbers k_1 and k_3 at early times (upper left and upper right, respectively) and after steady state has been reached (lower left and lower right, respectively). The mean gradient ('3' direction) is pointing in the vertical direction. It is apparent that at short times the topological shape of the $B(k,\mu)$ surface is similar to that for $Q_3(k,\mu)$, however, at long times, angular rearrangement occurs causing the autocorrelation spectrum to become nearly isotropic.

a factor $(1-l)$ fall into this category. By definition, these terms reinforce the anisotropy introduced by the source term.

The reason that $B_2(k) \neq -B_0(k)$ for all time is that some of the transfer terms in Eq. (29) [those with coefficients that are *not* proportional to $(1-l)$] redistribute the scalar in the *angular* direction of **k** space. The terms responsible for this angular redistribution are the ones associated with coefficients: G_6, G_7, M_3, and M_5. It should be noted that angular transfer is a conservative process; that is, the total root mean square fluctuation is conserved by the angular redistribution. Furthermore, the redistribution does not occur instantaneously, but requires a finite time to occur (approximately one eddy turnover time). This can be seen by considering the contour plots shown in Fig. 10. The upper left plot shows isocontours of the scalar autocorrelation $B(k,\mu)$ at a relatively short time $(t/T_e=0.1)$ plotted on the (k_1,k_3) plane (where the mean gradient points in the vertical direction). For the sake of comparison, the source term for $B(k,\mu)$ [Eq. (35)] is shown in the upper right. Equivalent plots of the scalar autocorrelation and source term at a later time $(t/T_e=33)$ are shown below. It is readily apparent that the source terms are strongly anisotropic at early and late times. (Note that an isotropic spectrum would appear as concentric circles in this diagram.) For example, none of the contours of either source term cross the k_3 axis. Likewise, the autocorrelation contours are strongly anisotropic at short times, particularly at small wave numbers (large scales), however, at longer times, the scalar contours form nearly perfect concentric circles (indicating near isotropy). Moreover, the contours are now slightly elongated *along the gradient axis*. This rearrangement in the contours explains why the ratio of derivatives shown in Fig. 6(b) starts out below unity (consistent with elongated contours in the transverse direction), but eventually ends up greater than unity as the scalar field rearranges. Note also that the rearrangement occurs most quickly at the highest wave numbers, and eventually proceeds to the lowest wave numbers. This is consistent with classical modeling arguments that assume rapid ''return to isotropy'' of the smallest scales.

Most of the published values for the relative ratio of derivatives were evaluated at several eddy turnover times,[2,6] long after the aforementioned rearrangement occurs, hence their values are always greater than unity. Initially, it was somewhat surprising to us that the ratio of derivatives could ever be greater than unity, based on the shape of the source term. The explanation appears to be that rapid angular rearrangement of the scalar occurs as a result of four of the transfer terms. The angular rearrangement is sufficiently fast

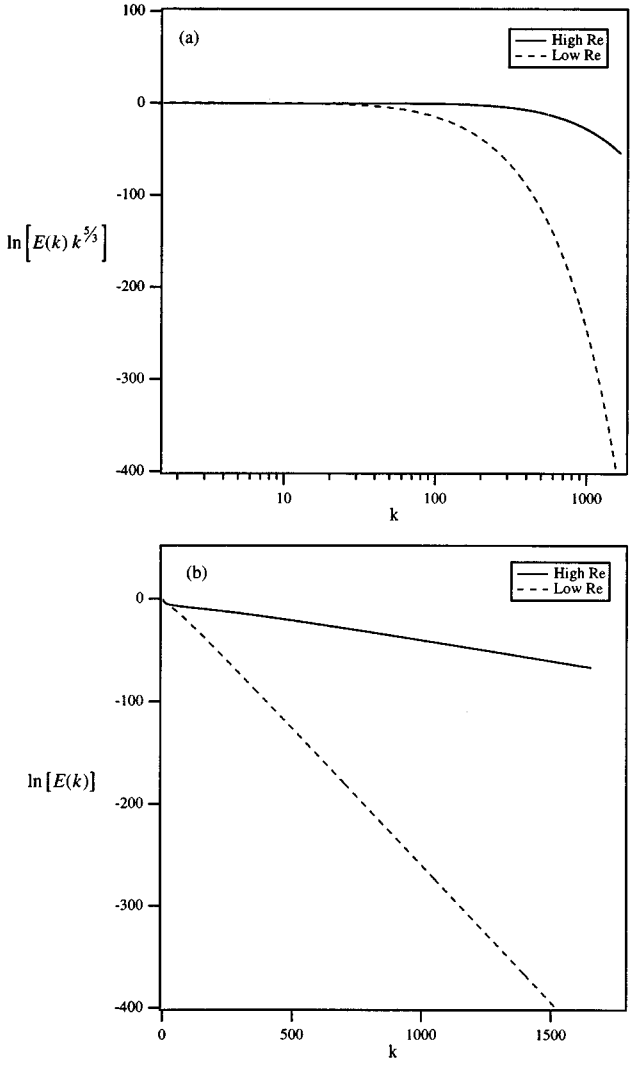

FIG. 11. (a) Energy spectrum for the high-resolution runs multiplied by $k^{5/3}$. The solid line corresponds to $R_\lambda=342$ and the dashed line corresponds to $R_\lambda=96$. Note the appearance of a well-defined inertial range (appears as a horizontal line in these coordinates). (b) Semilogarithmic plot of the energy spectrum that emphasizes the exponential behavior in the dissipation range of the spectrum.

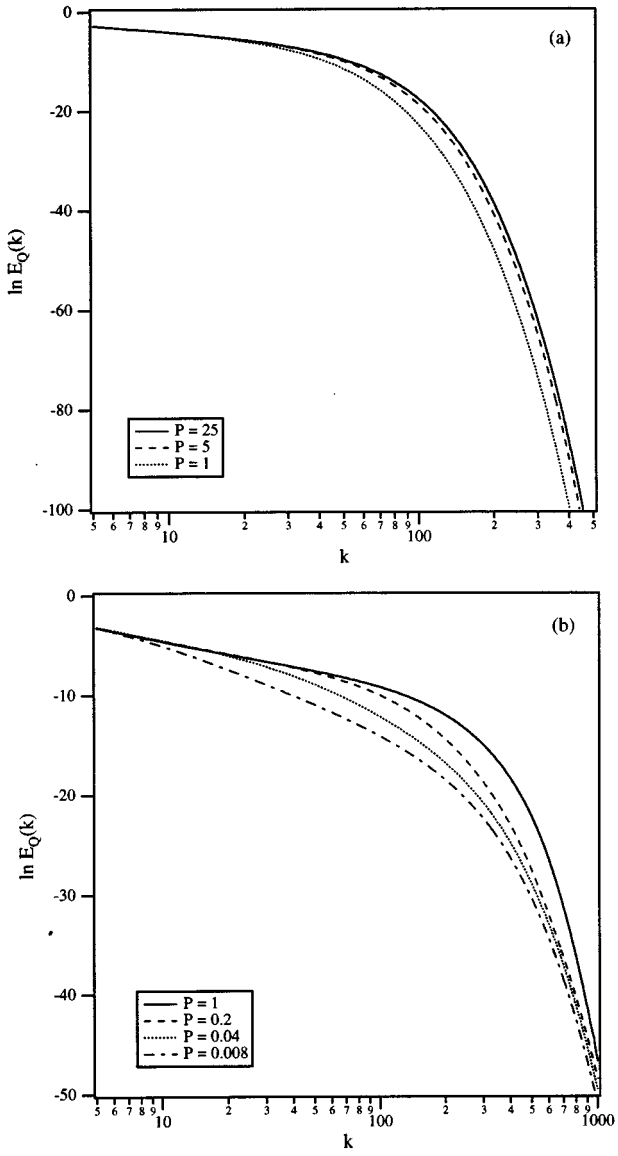

FIG. 12. The scalar-velocity cross-correlation spectrum $E_Q(k) = -k_2 Q(k)/3\pi^2$ as a function of wave number for the high-resolution number runs. (a) $R_\lambda=96$ and the Prandtl numbers are 25.0 (solid line), 5.0 (dashed line), and 1.0 (dotted line), respectively. (b) $R_\lambda=342$ and Prandtl numbers are 1.0 (solid line), 0.2 (dashed line), 0.04 (dotted line), and 0.008 (dash–dotted line), respectively.

that it erases all memory of the source term, yielding an autocorrelation spectrum that is nearly isotropic, and even slightly skewed in the direction of the mean gradient.

E. Model results at high Reynolds and Prandtl numbers

A major limitation with numerical simulations is the range of Reynolds numbers and Prandtl numbers that are numerically accessible. Models, in contrast, have no such limitation because the spectrum is fundamentally a one-dimensional (1-D) quantity (instead of a 3-D quantity); thus the storage requirements are substantially reduced. We have run the EDQNM model at Reynolds numbers of 96 and 342 (based on the Taylor Microscale) and Prandtl numbers ranging from 0.008 to 25. To accommodate these higher values, the maximum wave number was increased to 1024. Figure 11(a) shows the steady-state energy spectrum multiplied by $k^{5/3}$. A clear inertial range can be easily identified at both Reynolds numbers (note, the inertial range appears as a horizontal line in these coordinates). Figure 11(b) is a semilog plot of the energy spectrum to illustrate the exponential dissipation region that follows the inertial range. Note that at the highest Reynolds number, the inertial and dissipation ranges are distinct and well defined.

Figure 12(a) shows the steady-state cross-correlation spectrum $E_Q(k)\equiv -Q(k)k^2/3\pi^2$ at the lower Reynolds number and Prandtl numbers between 1 and 25, and Fig. 12(b) shows the same spectrum at the higher Reynolds number and Prandtl numbers ranging from 0.008 to 1. The Prandtl numbers were chosen to highlight the different scaling regions for the passive scalar. The spectra in both figures appear to have an inertial range followed by a dissipation range that depends on the Reynolds number and Prandtl

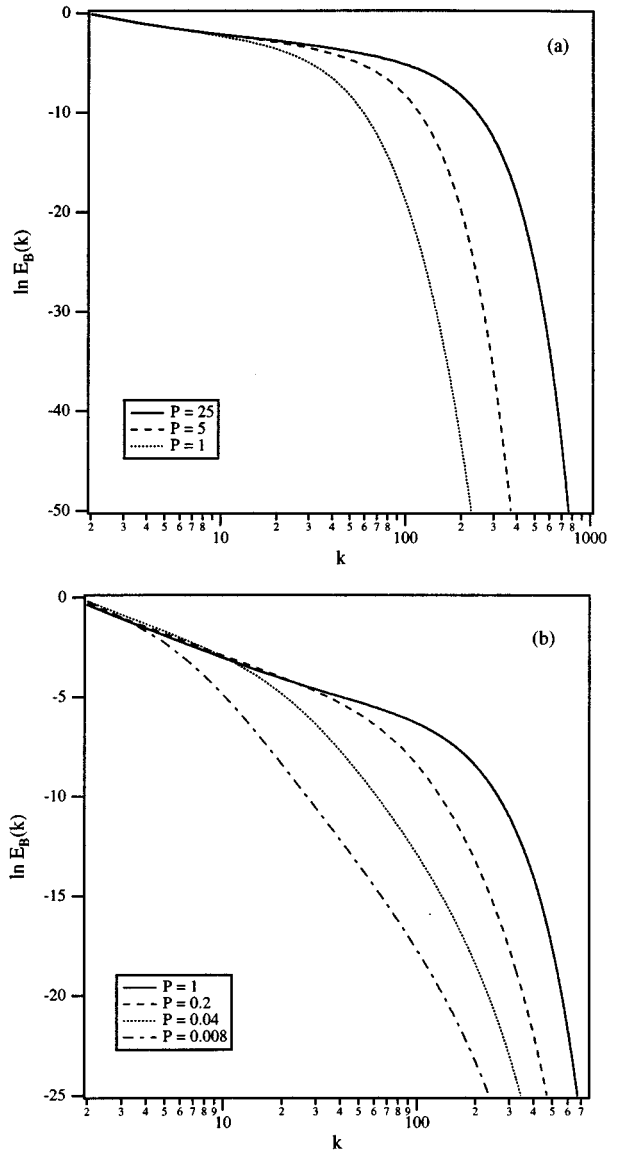

FIG. 13. The scalar autocorrelation spectrum $E_B(k)=k^2B_0(k)/\pi^2$ as a function of wave number for the high-resolution number runs. (a) $R_\lambda=96$ and the Prandtl numbers are 25.0 (solid line), 5.0 (dashed line), and 1.0 (dotted line), respectively. (b) $R_\lambda=342$ and Prandtl numbers are 1.0 (solid line), 0.2 (dashed line), 0.04 (dotted line), and 0.008 (dash–dotted line), respectively.

number. As expected, the location of the dissipation range in the spectrum moves to higher wave numbers with increasing Prandtl number, however, this will not continue indefinitely. At asymptotically large Prandtl numbers, the location of the dissipation range will be determined by the molecular viscosity, or in nondimensional terms, the Reynolds number. Thus, the cross-correlation spectrum must asymptotically become independent of the Prandtl number as the Prandtl number approaches infinity. This is evident in Fig. 12(a). Notice that the spectra at the two highest Prandtl numbers ($P=5$ and $P=25$) are much closer to each other than to the spectrum at the lowest Prandtl number ($P=1$).

The scalar autocorrelation spectrum $E_B(k) \equiv B_0(k)k^2/\pi^2$ is illustrated in Fig. 13 at both Reynolds numbers and the same Prandtl numbers, as shown in Fig. 12. For the low Reynolds number study [Fig. 13(a)], the scalar spectra have a well-defined inertial range with a $k^{-5/3}$ power law at low wave numbers followed by a second power-law region with a more shallow slope, and an exponential tail at very high wave numbers. The location of the dissipation range is a strong function of the Prandtl number. Once again, the dissipation range moves to higher wave numbers with increasing Prandtl number, however, in this case, the trend should continue indefinitely. That is, the autocorrelation spectrum will *not* approach a constant asymptotic shape at large values of the Prandtl number. Similar trends are observed in the high Reynolds number study [Fig. 13(b)]. Notice that the inertial range in the scalar spectrum at the lower Prandtl numbers is also followed by a second power-law region, however, now the slope of the second region is *steeper* than $k^{-5/3}$.

With the increased resolution of the present calculations, it is possible to quantitatively determine the scaling relationships within the ''second'' power-law region that follows the inertial range. We show the scalar autocorrelation spectra for the two limiting Prandtl numbers separately in Figs. 14(a) and 14(b), along with lines indicating the classical scaling laws. Figure 14(a) has a clear viscous-convective region with a k^{-1} power-law behavior, in agreement with the original analysis by Batchelor.[38] There has been an objection raised about the k^{-1} spectrum and the implicit logarithmic divergence of $\Phi_{\rm rms}$ as $P\to\infty$.[39] For the moment, we simply point out that the EDQNM model predicts a k^{-1} Batchelor region, even in the presence of a mean gradient. Furthermore, we note that this observation is consistent with, and perhaps partially explains, other experimental observations of k^{-1} Batchelor regions in more complex inhomogeneous flows.[40,41] Figure 14(b) shows the inertial-conductive range at the lowest Prandtl number with a dashed line indicating the classical $k^{-\frac{17}{3}}$ power law predicted by Batchelor *et al.*[42] Once again, there appears to be good agreement with the scaling law.

IX. CONCLUSIONS

An EDQNM turbulence transport model for a passive scalar in the presence of a uniform mean gradient has been developed. The model accounts for the axisymmetric scalar autocorrelation by expanding the angle dependence in a Legendre polynomial series. A fortuitous consequence of the initial conditions used in this study is that the infinite series can be rigorously truncated after the second term. The model contains two adjustable constants arising from the eddy damping procedure. Since there is no asymptotic form available for the scalar-velocity cross correlation, no external constraint could be placed on these coefficients, and consequently they were determined by optimizing the fit of the scalar-velocity cross correlation to the DNS results.

We compared a number of single-point statistics to the DNS database, including the scalar autocorrelation $\overline{\Phi'^2}$, scalar-velocity cross correlation $\overline{u_3\Phi'}$, and derivatives parallel and perpendicular to the mean scalar gradient. The agreement between the simulations and model was good for the scalar-velocity cross correlation, however, this can be partially attributed to the adjusted coefficients in the model. A

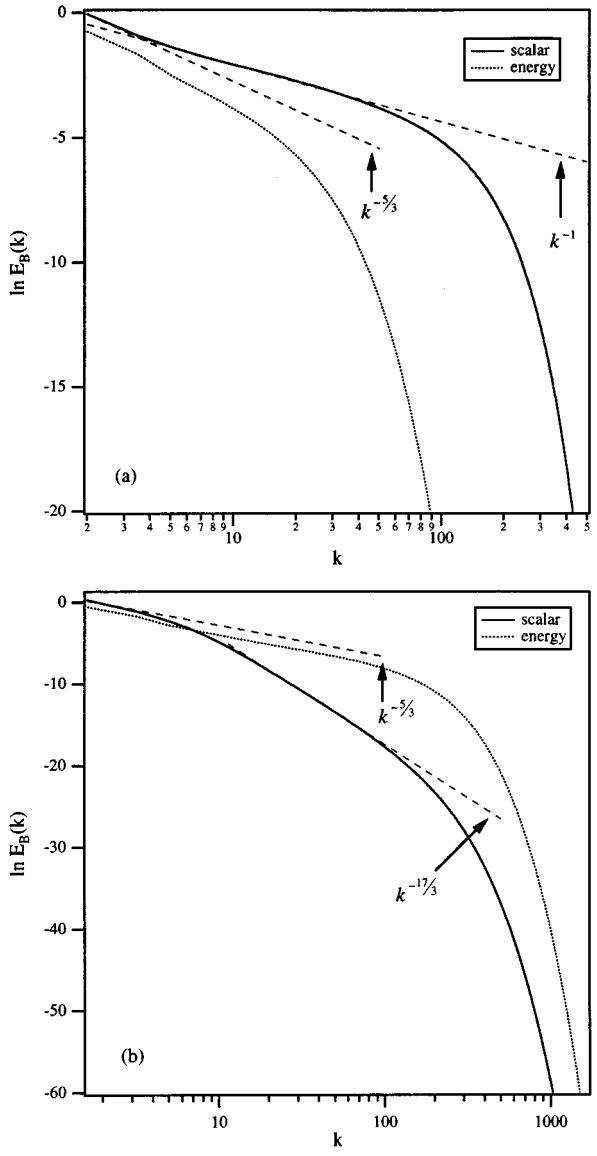

FIG. 14. Replot of the scalar autocorrelation spectra corresponding to the extreme values of the Prandtl number. (a) $P=25.0$ and (b) $P=0.008$. The dashed lines indicate the classical power-law behaviors for the different regimes, with the exponents as indicated on the graph. The energy spectrum is also shown for comparison (dotted line).

perhaps more stringent test was the scalar autocorrelation, which had no adjustable parameters in its equation (aside from those prescribed in earlier isotropic studies). Once again, we found the agreement between the model and simulations to be quite good (within 4%).

Earlier experimental and numerical studies of a passive scalar with a mean gradient reported differences in the magnitudes of scalar derivatives in directions parallel and perpendicular to the mean gradient, i.e., they found the scalar field to be anisotropic.[2,6] We likewise observed the same effect in the model, although the magnitude of the effect was smaller than that found in the other studies reported in the literature (approximately 8% for the ratio of the square of the parallel to perpendicular derivatives).

The presence and degree of anisotropy in the scalar field is extremely relevant to the development of a simplified model of scalar transport because incorporating anisotropy will add significantly to the model's complexity, ultimately limiting its utility for three-dimensional flows or flows in complex geometries. Remarkably, despite the strong anisotropy imposed on the scalar autocorrelation by the source terms, the scalar autocorrelation was found to be nearly isotropic after approximately one eddy turnover time. Apparently, the nonlinear transfer terms responsible for redistributing the scalar in wave number space also redistribute the scalar in the angular direction. This angular redistribution occurs sufficiently rapidly that the anisotropy imposed by the source term is completely negated by angular transfer. Indeed, we predicted the scalar spectrum to be slightly *enhanced* along the direction of the mean gradient at long times, in contrast to the source term that is identically zero along that direction (a result consistent with earlier experimental measurements in the literature). More importantly, our model and DNS results showed this difference to be quite small. We therefore conclude that given the significant errors in most single-point transport models introduced by the closure approximations, the error due to assuming local isotropy is most likely not as significant.

Comparisons of the spherically averaged spectra for the scalar-velocity cross correlation and scalar autocorrelation were made with the DNS results. In general, there was very good agreement between the two. There was excellent agreement within the inertial range, and some disagreement within the dissipation range. It is difficult to pinpoint the cause of the discrepancy at the higher wave numbers, particularly given the large number of transfer terms in the model (see Tables I and II). Perhaps a more systematic study of each transfer term may indicate the terms for which the EDQNM approximation is breaking down.

One advantage the EDQNM model has over DNS is that it is fundamentally one dimensional, thus it can be run at much higher Reynolds numbers and Prandtl numbers than can be achieved in the simulations. The high Reynolds number and Prandtl number studies allowed us to look for power-law scaling relationships for different ranges in the scalar autocorrelation spectrum. We observed a k^{-1} power law in the viscous-convective region at high Prandtl numbers (i.e., the so-called Batchelor region) and a $k^{-17/3}$ power law in the inertial-conductive range at very low Prandtl numbers. It was noted that there has been some controversy about the k^{-1} Batchelor region and its implications on the boundedness of Φ_{rms} in the limit $P\to\infty$. For the moment we only point out that the EDQNM model clearly predicts scaling consistent with the original Batchelor argument. A more comprehensive discussion of the Batchelor region will be the topic of a future paper.

ACKNOWLEDGMENTS

We acknowledge computational support for the simulations presented in this paper from Los Alamos National Laboratories. Two of the authors (SH and LRC) gratefully acknowledge financial support from Dow Chemical through the Young Minority Investigator Award (awarded to LRC).

APPENDIX A: DERIVATION OF THE CLOSED TRIPLE CORRELATIONS USING THE EDQNM APPROXIMATIONS

1. T_{jn}(k,p,q)

EDQNM theory provides a methodology for obtaining approximate relationships for the triple correlations such as $T_{jn}(\mathbf{k},\mathbf{p},\mathbf{q})$ based on the principle that the velocity and scalar fluctuations are nearly Gaussian. The theory involves three basic steps: (i) derive exact transport equations for unknown triple correlations; (ii) apply the quasinormal approximation to the fourth-order moments; and (iii) add eddy damping terms and apply the Markovian approximation to obtain an explicit expression for triple correlation.

The exact transport equation for $T_{jn}(\mathbf{x}_1,\mathbf{x}_2,\mathbf{x}_3)$ is as follows:

$$\left(\frac{\partial}{\partial t}-\mathrm{Pe}^{-1}\ \nabla_3^2-R_L^{-1}(\nabla_1^2+\nabla_2^2)\right)T_{jn}(\mathbf{x}_1,\mathbf{x}_2,\mathbf{x}_3)$$
$$=-\tfrac{1}{2}P_{nkl}(\mathbf{x}_2)T_{klj}(\mathbf{x}_2,\mathbf{x}_2,\mathbf{x}_1,\mathbf{x}_3)$$
$$-\tfrac{1}{2}P_{jkl}(\mathbf{x}_1)T_{kln}(\mathbf{x}_1,\mathbf{x}_1,\mathbf{x}_2,\mathbf{x}_3)$$
$$-\frac{\partial}{\partial x_{3l}}T_{jln}(\mathbf{x}_1,\mathbf{x}_3,\mathbf{x}_2,\mathbf{x}_3)-R_{j3n}(\mathbf{x}_1,\mathbf{x}_3,\mathbf{x}_2), \qquad \text{(A1a)}$$

where

$$T_{inj}(\mathbf{x}_1,\mathbf{x}_2,\mathbf{x}_3,\mathbf{x}_4)=\overline{u_i(\mathbf{x}_1)u_n(\mathbf{x}_2)u_j(\mathbf{x}_3)\Phi'(\mathbf{x}_4)}, \qquad \text{(A1b)}$$

$$R_{ijn}(\mathbf{x}_1,\mathbf{x}_2,\mathbf{x}_3)=\overline{u_i(\mathbf{x}_1)u_j(\mathbf{x}_2)u_n(\mathbf{x}_3)}. \qquad \text{(A1c)}$$

According to the EDQNM theory, $T_{inj}(\mathbf{x}_1,\mathbf{x}_2,\mathbf{x}_3,\mathbf{x}_4)$ can be approximated by

$$T_{inj}(\mathbf{x}_1,\mathbf{x}_2,\mathbf{x}_3,\mathbf{x}_4)\approx R_{in}(\mathbf{x}_1,\mathbf{x}_2)Q_j(\mathbf{x}_3,\mathbf{x}_4)$$
$$+R_{ij}(\mathbf{x}_1,\mathbf{x}_3)Q_n(\mathbf{x}_2,\mathbf{x}_4)$$
$$+R_{nj}(\mathbf{x}_2,\mathbf{x}_3)Q_i(\mathbf{x}_1,\mathbf{x}_4). \qquad \text{(A2)}$$

Upon substituting this approximation into Eq. (A1a), Fourier Transforming, and taking advantage of the known tensorial relationships for the lower-order moments, the following expression is obtained:

$$\left(\frac{\partial}{\partial t}+\mathrm{Pe}^{-1}\ q^2+R_L^{-1}(k^2+p^2)\right)T_{jn}(\mathbf{k},\mathbf{p},\mathbf{q})=-i\hat{\delta}(\mathbf{k}+\mathbf{p}+\mathbf{q})\Big[q_lP_{jl}(\mathbf{k})P_{n3}(\mathbf{p})R(k)Q(p)+q_lP_{ln}(\mathbf{p})P_{j3}(\mathbf{k})R(p)Q(k)$$
$$+\frac{1}{2}P_{nkl}(\mathbf{p})P_{kj}(\mathbf{k})P_{13}(\mathbf{q})R(k)Q(q)+\frac{1}{2}P_{nkl}(\mathbf{p})P_{lj}(\mathbf{k})P_{k3}(\mathbf{q})R(k)Q(q)$$
$$+\frac{1}{2}P_{jkl}(\mathbf{k})P_{kn}(\mathbf{p})P_{13}(\mathbf{q})R(p)Q(q)+\frac{1}{2}P_{jkl}(\mathbf{k})P_{ln}(\mathbf{p})P_{k3}(\mathbf{q})R(p)Q(q)\Big]$$
$$+R_{j3n}(\mathbf{k},\mathbf{q},\mathbf{p}). \qquad \text{(A3)}$$

The expression for R_{j3n} $(\mathbf{k},\mathbf{q},\mathbf{p})$, determined previously for the energy equation,[28] can be used in Eq. (A3). Of course, since the energy field is not evolving in time (stationary turbulence), $R_{j3n}(\mathbf{k},\mathbf{q},\mathbf{p})$ is constant. Equation (A3) can be formally solved for $T_{jn}(\mathbf{k},\mathbf{p},\mathbf{q})$ in terms of a time integral over the right-hand side. Introducing the standard eddy damping terms and invoking the Markovianization approximation[28] yields the following explicit relationship for $T_{jn}(\mathbf{k},\mathbf{p},\mathbf{q})$:

$$T_{jn}(\mathbf{k},\mathbf{p},\mathbf{q})=-i\hat{\delta}(\mathbf{k}+\mathbf{p}+\mathbf{q})\Theta_T^{kpq}\{-\Theta_R^{kqp}[D_{3jn}^{qkp}R(k)R(p)$$
$$+D_{nj3}^{pkq}R(k)R(q)+D_{j3n}^{kqp}R(p)R(q)]$$
$$+C_{nj}^{qpk}R(p)Q(k)+D_{n3j}^{pqk}R(k)Q(q)$$
$$+D_{jn3}^{kpq}R(p)Q(q)+C_{jn}^{qkp}R(k)Q(p)\}. \qquad \text{(A4)}$$

Definitions for Θ_R^{kpq} and Θ_T^{kpq} are given in Eqs. (11d) and (17d) in the main text, and the compact notation defined in Eqs. (17b) and (17c) is being used.

2. M_n(q,k,p)

The transport equation for $M_n(\mathbf{x}_3,\mathbf{x}_1,\mathbf{x}_2)$ in physical space is shown below:

$$\left(\frac{\partial}{\partial t}-\mathrm{Pe}^{-1}(\nabla_1^2+\nabla_3^2)-R_L^{-1}\nabla_2^2\right)M_n(\mathbf{x}_2,\mathbf{x}_1,\mathbf{x}_3)$$
$$=-\frac{\partial}{\partial x_{1j}}M_{nj}(\mathbf{x}_2,\mathbf{x}_1,\mathbf{x}_1,\mathbf{x}_3)-\frac{\partial}{\partial x_{3j}}M_{nj}(\mathbf{x}_2,\mathbf{x}_3,\mathbf{x}_1,\mathbf{x}_3)$$
$$-\frac{\partial}{\partial x_{2i}}P_{nj}(\mathbf{x}_3)M_{ji}(\mathbf{x}_2,\mathbf{x}_2,\mathbf{x}_1,\mathbf{x}_3)-T_{n3}(\mathbf{x}_2,\mathbf{x}_1,\mathbf{x}_3)$$
$$-T_{n3}(\mathbf{x}_2,\mathbf{x}_3,\mathbf{x}_1), \qquad \text{(A5a)}$$

where

$$M_{in}(\mathbf{x}_1,\mathbf{x}_2,\mathbf{x}_3,\mathbf{x}_4)=\overline{u_i(\mathbf{x}_1)u_n(\mathbf{x}_2)\Phi'(\mathbf{x}_3)\Phi'(\mathbf{x}_4)}. \quad \text{(A5b)}$$

The quasinormal approximation for $M_{in}(\mathbf{x}_1,\mathbf{x}_2,\mathbf{x}_3,\mathbf{x}_4)$ is given by

$$\begin{aligned}M_{in}(\mathbf{x}_1,\mathbf{x}_2,\mathbf{x}_3,\mathbf{x}_4)\approx{}&R_{in}(\mathbf{x}_1,\mathbf{x}_2)B(\mathbf{x}_3,\mathbf{x}_4)\\&+Q_i(\mathbf{x}_1,\mathbf{x}_3)Q_n(\mathbf{x}_2,\mathbf{x}_4)\\&+Q_i(\mathbf{x}_1,\mathbf{x}_4)Q_n(\mathbf{x}_2,\mathbf{x}_3).\end{aligned} \quad \text{(A6)}$$

Substituting into Eq. (A5) and Fourier transforming the resulting equation yields

$$\begin{aligned}\left(\frac{\partial}{\partial t}+\mathrm{Pe}^{-1}(k^2+q^2)+R_L^{-1}p^2\right)M_n(\mathbf{p},\mathbf{k},\mathbf{q})=&-i\hat{\delta}(\mathbf{k}+\mathbf{p}+\mathbf{q})[q_aP_{3a}(\mathbf{k})P_{i3}(\mathbf{p})Q(k)Q(p)\\&+\tfrac{1}{2}P_{iab}(\mathbf{p})P_{a3}(\mathbf{k})P_{b3}(\mathbf{q})Q(k)Q(q)+\tfrac{1}{2}P_{iab}(\mathbf{p})P_{a3}(\mathbf{q})P_{b3}(\mathbf{k})Q(k)Q(q)\\&+k_aP_{3a}(\mathbf{q})P_{i3}(\mathbf{p})Q(p)Q(q)+2q_aP_{ia}(\mathbf{p})R(p)B(k,\mu)\\&+2k_aP_{ia}(\mathbf{p})R(p)B(q,\mu'')]-T_{n3}(\mathbf{p},\mathbf{k},\mathbf{q})-T_{n3}(\mathbf{p},\mathbf{q},\mathbf{k}).\end{aligned} \quad \text{(A7)}$$

Standard eddy damping coefficients can now be introduced into Eq. (A7). The Markovian approximation, in contrast, is complicated by the fact that $T_{n3}(\mathbf{p},\mathbf{k},\mathbf{q})$ and $T_{n3}(\mathbf{p},\mathbf{q},\mathbf{k})$ are exponential functions of time, from the previous Markovian approximation. Consequently, ''Markovianization'' of Eq. (A7) shall neglect the time variation of the scalar spectra, as is usually done, but will account for the exponential functions introduced by the previous Markovian approximations in $T_{n3}(\mathbf{p},\mathbf{k},\mathbf{q})$ and $T_{n3}(\mathbf{p},\mathbf{q},\mathbf{k})$. The result is

$$\begin{aligned}M_n(\mathbf{p},\mathbf{k},\mathbf{q})=&-i\hat{\delta}(\mathbf{k}+\mathbf{p}+\mathbf{q})(-\Theta_{M'}^{pkq;pkq}\{-\Theta_R^{pqk}[D_{3n3}^{qpk}R(k)R(p)+D_{n33}^{pqk}R(k)R(q)+D_{3n3}^{kpq}R(p)R(q)]+C_{n3}^{qpk}R(p)Q(k)\\&+C_{3n}^{qkp}R(k)Q(p)+D_{n33}^{pkq}R(k)Q(q)+D_{33n}^{kqp}R(p)Q(q)\}-\Theta_{M'}^{pkq;pqk}\{-\Theta_R^{pkq}[D_{3n3}^{qpk}R(k)R(p)+D_{n33}^{pkq}R(k)R(q)\\&+D_{3n3}^{kpq}R(p)R(q)]+D_{33n}^{qkp}R(p)Q(k)+D_{n33}^{pqk}R(q)Q(k)+C_{3n}^{kqp}R(q)Q(p)+C_{n3}^{kpq}R(p)Q(q)\}\\&+\Theta_M^{pkq}[C_{3n}^{qkp}Q(k)Q(p)+D_{n33}^{pkq}Q(k)Q(q)+C_{3n}^{kqp}Q(p)Q(q)+A_n^{qp}R(p)B(k,\mu)+A_n^{kp}R(p)B(q,\mu'')]).\end{aligned} \quad \text{(A8)}$$

Expressions for the new eddy damping coefficients are given in Eqs. (25c) and (25d) in the main text.

APPENDIX B: GEOMETRIC CONSIDERATIONS IN EVALUATING THE CONVOLUTION INTEGRAL

The expressions for $T_{jn}(\mathbf{k},\mathbf{p},\mathbf{q})$ and $M_n(\mathbf{p},\mathbf{k},\mathbf{q})$ [Eqs. (17a) and (25a)] in principle, can be substituted into Eqs. (16) and (24) to obtain closed relationships for $B(k,\mu)$ and $Q(k)$, however, it is important to first consider precisely how the convolution integral is to be evaluated. Homogeneity ensures that all triple correlations are proportional to $\hat{\delta}(\mathbf{k}+\mathbf{p}+\mathbf{q})$, thus the convolution integrals can be thought of as having the following generic form:

$$\frac{1}{(2\pi)^6}\int\int F(k,p,q,\mu,\mu',\mu'')\hat{\delta}(\mathbf{k}+\mathbf{p}+\mathbf{q})d\mathbf{p}\,d\mathbf{q}, \quad \text{(B1)}$$

where μ, μ', and μ'' are the cosines of the angles between the wave vectors $\mathbf{k}$, $\mathbf{p}$, and $\mathbf{q}$ and the mean gradient $\mathbf{e}_3$, respectively. In an earlier study of turbulence with mean shear, Nakauchi[24] introduced an alternative coordinate system for evaluating the convolution integral. The standard one, referred to as $(\mathbf{e}_1,\mathbf{e}_2,\mathbf{e}_3)$, is the coordinate system aligned with the mean gradient. The alternative coordinate system, referred to as $(\mathbf{e}_1',\mathbf{e}_2',\mathbf{e}_3')$ and shown schematically in Fig. 15, is positioned such that the vector $\mathbf{k}$ is aligned with $\mathbf{e}_3'$. The motivation for introducing the second coordinate system is that the convolution integral can be more easily evaluated in that system. One complication of axisymmetric turbulence is that the geometric factors A_i^{kp}, C_{ij}^{kpq}, and D_{ijm}^{kpq} will depend on the internal angles of the triad and the angle of the wave vectors to the mean gradient. Thus, relationships for expressing the angles μ, μ', and μ'' in the $(\mathbf{e}_1',\mathbf{e}_2',\mathbf{e}_3')$ coordinate system are required. By design the angle μ remains unchanged. Nakauchi[24] derived the following relationships for μ' and μ'':

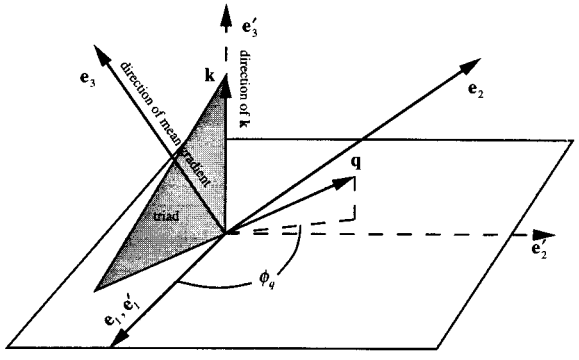

FIG. 15. Coordinate systems for evaluating the convolution integral. ($\mathbf{e}_1$, $\mathbf{e}_2$, $\mathbf{e}_3$) is the natural coordinate system based on the direction of the mean gradient, while $(\mathbf{e}_1',\mathbf{e}_2',\mathbf{e}_3')$ is chosen so that $\mathbf{e}_3'$ is aligned with the $\mathbf{k}$ vector. The latter coordinate system is used to evaluate the convolution integral because it simplifies the integrand.

$$\mu' = -\mu z - \sqrt{(1-\mu^2)(1-z^2)}\sin\,\phi_q, \tag{B2a}$$

$$\mu'' = -\mu y + \sqrt{(1-\mu^2)(1-y^2)}\sin\,\phi_q, \tag{B2b}$$

where ϕ_q is the angle of the projection of $\mathbf{q}$ onto the $\mathbf{e}_1' - \mathbf{e}_2'$ plane (see Fig. 15 for details).

Returning to the convolution integral shown in Eq. (B1), we can now integrate with respect to the $\mathbf{p}$ vector, yielding

$$\frac{1}{(2\pi)^3}\int F(k,|\mathbf{k}+\mathbf{q}|,q,\mu,\mu',\mu'')q^2 d\,\cos\,\theta_q d\phi_q\,dq. \tag{B3}$$

From geometric considerations one can show that $d\,\cos\,\theta_q = (p/qk)dp$, thus the integral becomes

$$\frac{1}{(2\pi)^3}\int_\Delta F(k,p,q,\mu,\mu',\mu'')\,\frac{pq}{k}\,dp\,dq\,d\phi_q, \tag{B4}$$

where the symbol Δ indicates an integration over triads. For an isotropic system the integral over $d\phi_q$ simply introduces a factor of 2π, however, the integrand in an axisymmetric system can depend on the angle ϕ_q. In all cases the angle integration with respect to ϕ_q was done analytically, producing geometric coefficients that were functions of the magnitudes of k, p, and q only. (Note: the *interior* angles of the triad can be related to the magnitudes of the wave vectors through the law of cosines.) Thus, the integral is ultimately reduced to the following generic form

$$\frac{1}{(2\pi)^3}\int_\Delta F'(k,p,q,\mu)\,\frac{pq}{k}\,dp\,dq, \tag{B5}$$

where the modified coefficient $F'(k,p,q,\mu)$ is the result from the angle integration over $d\phi_q$. The angle integration will yield a different coefficient for each term in the convolution integral, hence there will be a large number of coefficients, however, this introduces no additional complexity, aside from bookkeeping, because all coefficients can be evaluated analytically. Furthermore, it should be noted that the final *numerical* integration is only over the wave numbers p and q, much like the isotropic system, thus remarkably the extension to axisymmetry does not introduce any additional computational burden or inaccuracy over that for the isotropic system.

[1] C. Tong and Z. Warhaft, ''Passive scalar dispersion and mixing in a turbulent jet,'' J. Fluid Mech. **292**, 1 (1995).
[2] C. Tong and Z. Warhaft, ''On passive scalar derivative statistics in grid turbulence,'' Phys. Fluids **6**, 2165 (1994).
[3] Jayesh, C. Tong, and Z. Warhaft, ''On temperature spectra in grid turbulence,'' Phys. Fluids **6**, 306 (1994).
[4] Jayesh and Z. Warhaft, ''Probability distribution, conditional dissipation, and transport of passive temperature fluctuations in grid-generated turbulence,'' Phys. Fluids A **4**, 2292 (1992).
[5] Jayesh and Z. Warhaft, ''Probability distribution of a passive scalar in grid-generated turbulence,'' Phys. Rev. Lett. **67**, 3503 (1991).
[6] A. Pumir, ''A numerical study of the mixing of a passive scalar in three dimensions in the presence of a mean gradient,'' Phys. Fluids **6**, 2118 (1994).
[7] A. Pumir, B. Shraiman, and E. D. Siggia, ''Exponential tails and random advection,'' Phys. Rev. Lett. **66**, 2984 (1991).
[8] J. P. Gollub, J. Clarke, M. Gharib, B. Lane, and O. N. Mesquita, ''Fluctuations and transport in a stirred fluid with a mean gradient,'' Phys. Rev. Lett. **67**, 3507 (1991).
[9] M. M. Rogers, ''The structure of a passive scalar field with a uniform mean gradient in rapidly sheared homogeneous turbulent flow,'' Phys. Fluids A **3**, 144 (1991).
[10] J. R. Chasnov, ''Similarity states of passive scalar transport in isotropic turbulence,'' Phys. Fluids **6**, 1036 (1994).
[11] S. Tavoularis and S. Corrsin, ''Experiments in nearly homogeneous turbulent shear flow with a uniform mean temperature gradient. Part 1,'' J. Fluid Mech. **104**, 311 (1981).
[12] S. Tavoularis and S. Corrsin, ''Experiments in nearly homogeneous turbulent shear flow with a uniform mean temperature gradient. Part 2. The fine structure,'' J. Fluid Mech. **104**, 349 (1981).
[13] A. N. Kolmogorov, ''The local structure of turbulence in incompressible fluid at very high Reynolds number,'' Dokl. Acad. Sci. USSR **30**, 299 (1941).
[14] A. M. Obukhov, ''Structure of the temperature field in turbulent flows,'' Izv. Akad. Nauk SSSR, Geogmagn and Geophys. Ser. **13**, 58 (1949).
[15] S. Corrsin, ''On the spectrum of isotropic temperature fluctuations in isotropic turbulence,'' J. Appl. Phys. **22**, 469 (1951).
[16] K. R. Sreenivasan, ''On local isotropy of passive scalar in turbulent shear flows,'' Proc. R. Soc. London Ser. A **434**, 165 (1991).
[17] R. R. Prasad and K. R. Sreenivasan, ''Quantitative three-dimensional imaging and the structure of passive scalar fields in fully turbulent flows,'' J. Fluid Mech. **216**, 1 (1990).
[18] S. A. Orszag, ''Analytical theories of turbulence,'' J. Fluid Mech. **41**, 363 (1970).
[19] J. R. Herring, D. Schertzer, M. Lesieur, G. R. Newman, J. P. Chollet, and M. Larcheveque, ''A comparative assessment of spectral closures as applied to passive scalar diffusion,'' J. Fluid Mech. **124**, 411 (1982).
[20] M. Lesieur and J. Herring, ''Diffusion of a passive scalar in two-dimensional turbulence,'' J. Fluid Mech. **161**, 77 (1985).
[21] N. Nakauchi, H. Oshima, and Y. Saito, ''A passive scalar convected by homogeneous axisymmetric turbulence,'' Phys. Fluids A **1**, 723 (1989).
[22] N. Nakauchi and S. Sega, ''The homogeneous axisymmetric passive scalar in isotropic turbulence,'' Phys. Fluids **30**, 337 (1987).
[23] N. Nakauchi and H. Oshima, ''The return of strongly anisotropic turbulence to isotropy,'' Phys. Fluids **30**, 3653 (1987).
[24] N. Nakauchi, ''An application of the modified zero-fourth-cumulant approximation to homogeneous axisymmetric turbulence,'' J. Phys. Soc. Jpn. **53**, 1682 (1984).
[25] J. R. Herring, ''Approach of axisymmetric turbulence to isotropy,'' Phys. Fluids **17**, 859 (1974).
[26] G. K. Batchelor, ''The theory of axisymmetric turbulence,'' Proc. R. Soc. London Ser. A **186**, 480 (1946).
[27] S. Chandrasekhar, Philos. Trans. Ser. A **242**, 557 (1950).
[28] M. Lesieur, *Turbulence in Fluids*, 2nd ed. (Nijhoff, Boston, MA, 1987).
[29] J. C. Andre and M. Lesieur, ''Influence of helicity on the evolution of isotropic turbulence at high Reynolds number,'' J. Fluid Mech. **81**, 187 (1977).
[30] S. Herr, ''Modeling the behavior of a passive scalar with a uniform mean gradient in isotropic turbulence,'' MS thesis, The Pennsylvania State University, 1996.
[31] L.-P. Wang, S. Chen, J. G. Brasseur, and J. C. Wyngaard, ''Examination of hypotheses in Kolmogorov refined turbulence theory through high-resolution simulations. I. Velocity field,'' J. Fluid Mech. (in press).
[32] L.-P. Wang, S. Chen, J. G. Brasseur, and J. C. Wyngaard, ''Examination of hypotheses in Kolmogorov refined turbulence theory through high-resolution simulations. II. Passive scalar field,'' J. Fluid Mech. (in review) (1995).
[33] S. Chen and X. Shan, ''High resolution turbulence simulations using the connection machine—2,'' Comput. Phys. **6**, 643 (1992).
[34] C. Canuto, M. Y. Hussaini, A. Quarteroni, and T. A. Zang, *Spectral Methods in Fluid Dynamics* (Springer-Verlag, New York, 1988).
[35] G. R. Ruetsch and M. R. Maxey, ''Small-scale features of vorticity and passive scalar fields in homogeneous isotropic turbulence,'' Phys. Fluids A **3**, 1587 (1991).
[36] V. Eswaran and S. B. Pope, ''An examination of forcing in direct numerical simulations of turbulence,'' Comput. Fluids **16**, 257 (1988).
[37] J. G. Brasseur and C.-H. Wei, ''Interscale dynamics and local isotropy in high Reynolds number turbulence within triadic interactions,'' Phys. Fluids **6**, 842 (1994).
[38] G. K. Batchelor, ''Small-scale variation of convected quantities like temperature in turbulent fluid. Part 1. General discussion and the case of small conductivity,'' J. Fluid Mech. **5**, 113 (1959).
[39] P. E. Dimotakis and P. L. Miller, ''Some consequences of the boundedness of scalar fluctuations,'' Phys. Fluids A **2**, 1919 (1990).

[40]R. R. Prasad and K. R. Sreenivasan, ''The measurement and interpretation of fractal dimensions of the scalar interface in turbulent flows,'' Phys. Fluids A **2**, 792 (1990).
[41]K. B. Southerland, W. J. A. Dahm, and D. R. Dowling, *Experimental Results for the High Wavenumber Spectral Structure of Scalar Mixing in Turbulent Shear Flows*, in 10th Symposium on Turbulent Shear Flows (The Pennsylvania State University, State College, PA, 1995).
[42]G. K. Batchelor, I. D. Howells, and A. A. Townsend, ''Small-scale variation of convected quantities like temperature in turbulent fluid. Part 2. The case of large conductivity,'' J. Fluid Mech. **5**, 134 (1959).